Region-specific regulation of stem cell-driven regeneration in tapeworms.

Tania Rozario[1*], Edward B. Quinn[1], Jianbin Wang[2], Richard E. Davis[2], and Phillip A. Newmark[1,3,4*]

[1]Morgridge Institute for Research, Madison, WI, USA, [2]Department of Biochemistry and Molecular Genetics, RNA Bioscience Initiative, University of Colorado School of Medicine, Aurora, CO, USA, [3]Howard Hughes Medical Institute, [4]Department of Integrative Biology, University of Wisconsin-Madison, Madison, WI, USA.

* corresponding authors

Email: pnewmark@morgridge.org

trozario@morgridge.org

Abstract

Tapeworms grow at rates rivaling the fastest-growing metazoan tissues. To propagate they shed large parts of their body; to replace these lost tissues they regenerate proglottids (segments) as part of normal homeostasis. Their remarkable growth and regeneration are fueled by adult somatic stem cells that have yet to be characterized molecularly. Using the rat intestinal tapeworm, *Hymenolepis diminuta*, we find that regenerative potential is regionally limited to the neck, where head-dependent extrinsic signals create a permissive microenvironment for stem cell-driven regeneration. Using transcriptomic analyses and RNA interference, we characterize and functionally validate regulators of tapeworm growth and regeneration. We find no evidence that stem cells are restricted to the regeneration-competent neck. Instead, lethally irradiated tapeworms can be rescued when cells from either regeneration-competent or regeneration-incompetent regions are transplanted into the neck. Together, the head and neck tissues provide extrinsic cues that regulate stem cells, enabling region-specific regeneration in this parasite.

Introduction

Tapeworms are parasitic flatworms that infect humans and livestock, causing lost economic output, disease, and in rare cases, death[1]. These parasites are well known for their ability to reach enormous lengths. For example, humans infected with the broad or fish tapeworm, *Diphyllobothrium latum*, harbor parasites that average 6 m in length[2]. It is less commonly appreciated that tapeworms can regenerate to accommodate their multi-host life cycle. Adult tapeworms in their host intestines develop proglottids (segments) that are gravid with embryos. Tapeworms pinch off the posterior and gravid sections of their body, which exit with the host excrement, to be eaten by a suitable intermediate host that supports larval tapeworm development. Despite losing large body sections, the tapeworm does not progressively shorten; instead, it regenerates proglottids, allowing the worms to maintain an equilibrium length. Despite this remarkable biology, tapeworms are an unexplored animal model in the study of regenerative behaviors.

Up to the 1980s the rat intestinal tapeworm, *Hymenolepis diminuta*, had been a favorite model organism among parasitologists. *H. diminuta* grows rapidly–within the first 15 days of infection, it produces up to 2200 proglottids, increases in length by up to 3400 times, and weight by up to 1.8 million times[3]–and is easily propagated in the laboratory. Foundational work on their biochemistry, ultrastructure, and developmental biology enriched our understanding of these tapeworms[4]. However, with the dawn of the molecular age and the rise of genetic model organisms, *H. diminuta* was essentially left behind. Here, we show that *H. diminuta* is an excellent, tractable model for the study of stem cells and regeneration, with the power to inform us about parasite physiology.

50 As an obligate endoparasite, adult *H. diminuta* will expire once its host rat dies. However,
51 the lifespan of *H. diminuta* can be greatly increased via regeneration. A single adult tapeworm can
52 be serially amputated and transplanted into a new host intestine, where the fragment can regenerate
53 into a mature tapeworm even after 13 rounds of amputation over 14 years[5]. These observations
54 have led to speculation that *H. diminuta* may be inherently immortal. This situation is reminiscent
55 of the free-living cousins of tapeworms: freshwater planarians like *Schmidtea mediterranea*, which
56 reproduce indefinitely by fission, and can regenerate their whole body from tiny fragments[6].
57 Planarian immortality and regeneration are enabled by adult somatic stem cells called
58 neoblasts[6-8]. These stem cells are the only dividing undifferentiated cells within the soma. Like
59 planarians, *H. diminuta* maintains a population of neoblast-like adult somatic stem cells[3] that are
60 likely responsible for their growth and regenerative ability. Recently, stem cells of multiple species
61 of parasitic flatworms have been described[9-13]. Stem cells play crucial roles in parasite
62 development, transmission, homeostasis, and even disease. For example, stem cells enable prolific
63 reproduction and longevity[14], mediate host-parasite interactions[15], and allow metastatic parasite
64 transmission in host tissues[16]. How stem cells may regulate regeneration in parasites such as
65 tapeworms is largely unexplored and the subject of this study.
66 We use *H. diminuta,* to investigate the molecular basis of tapeworm regeneration. We
67 have established and refined experimental tools such as transcriptomics, *in vitro* parasite culture,
68 whole-mount and fluorescent RNA *in situ* hybridization (WISH and FISH), cycling-cell tracing
69 with thymidine analogs, RNA interference (RNAi), and cell transplantation, all described in this
70 work. We determine that the ability to regenerate is regionally limited to the neck of adult *H.*
71 *diminuta*. However, regeneration from the neck is finite without signals from the tapeworm head.
72 Using RNA sequencing (RNA-seq), we identify and characterize various markers of the somatic

73 cycling-cell population, which includes tapeworm stem cells. Using RNAi, we functionally
74 validate molecular regulators of growth and regeneration. However, our analyses failed to
75 uncover a neck-specific stem cell population that explains the regional regenerative ability
76 displayed by *H. diminuta.* Instead, we show that cells from both regeneration-competent and
77 regeneration-incompetent regions of *H. diminuta* have stem cell ability and can restore viability
78 to lethally irradiated tapeworms. Our results show that extrinsic signals present in the tapeworm
79 neck, rather than specialized stem cells, confer region-specific regenerative ability in this
80 tapeworm.

Results

The anatomy of adult *H. diminuta* consists of a head with four suckers, an unsegmented neck, and a body with thousands of proglottids/segments that grow and mature in an anterior-to-posterior direction[3,17] (Fig. 1a). What regions of the tapeworm body are competent to regenerate? In order to test regeneration competency, it is necessary to grow tapeworms *in vitro* instead of in the intestine, where the suckers are required to maintain parasites *in vivo*. We established *H. diminuta in vitro* culture conditions modified from Schiller's method[18] and tested the regeneration competence of 1 cm amputated fragments (Fig. 1b-c). The anterior-most fragments (head+neck+body) were competent to regenerate, confirming *in vivo* observations using amputation and transplantation[5,19]. Anterior fragments that were first decapitated (neck+body) were also competent to regenerate. In contrast, "body only" fragments failed to regenerate proglottids. All amputated fragments could grow in length (Fig. 1d), differentiate mature reproductive structures, and mate. Despite the failure to regenerate, "body only" fragments could grow because each existing proglottid increased in length as it progressively matured (Fig. 1 – figure supplement 1a-b). However, only fragments that retained the neck were able to regenerate new proglottids over time. The neck of 6 day-old tapeworms used in this study is typically 2-3 mm long when observed after DAPI staining and widefield fluorescent microscopy. By amputating 2 mm "neck only" fragments, we find that the neck is sufficient to regenerate an average of 383 proglottids (SD=138, N=4, n=20) after 12 days *in vitro* (Fig. 1e). In no case did we observe head regeneration. Furthermore, amputated heads alone could not regenerate *in vitro* (Fig. 1 – figure supplement 1c) nor *in vivo*[5]. Thus, neither the head nor body can regenerate proglottids, but the neck is both necessary and sufficient for proglottid-specific regeneration in *H. diminuta*.

103 Previous *in vivo* studies have shown that *H. diminuta* can regenerate after serial rounds of
104 amputation and transplantation for over a decade[5] and perhaps indefinitely. Using *in vitro* culture,
105 we confirmed that anterior fragments of *H. diminuta* can regenerate after at least four rounds of
106 serial amputation (Fig. 1f-g). Decapitated (-head) fragments regenerated proglottids after the first
107 amputation; however, re-amputation abrogated regeneration (Fig. 1f-g). After decapitation, a
108 definitive neck could not be maintained and eventually, the whole tissue was comprised of
109 proglottids (Fig. 1–figure supplement 2). Without the head, proglottid regeneration from the neck
110 is finite. Thus, while the neck is necessary and sufficient for proglottid regeneration, the head is
111 required to maintain an unsegmented neck and for persistent regeneration.

112 If signals from the head regulate regeneration, is regenerative potential asymmetric across
113 the anterior-posterior (A-P) axis of the neck? We subdivided the neck into three 1 mm fragments
114 and found that the most-anterior neck fragments regenerated more proglottids than the middle or
115 posterior neck fragments (Fig. 1h-i). Thus, regeneration potential is asymmetric across the neck
116 A-P axis with a strong anterior bias.

117 Since the neck is the only region competent to regenerate, are stem cells preferentially
118 confined to the neck? In lieu of specific molecular markers for stem cells, we examined the
119 distribution of all cycling cells in adult tapeworms. In flatworms, it has been repeatedly shown that
120 the only proliferative cells are undifferentiated cells with stem cell morphology and/or function;
121 these cells have been termed neoblasts, adult somatic stem cells, or germinative cells, depending
122 on the organism[9,10,20-22]. In *H. diminuta,* proliferation does not occur in regions comprised solely
123 of differentiated cells (muscle and tegument/parasite skin at the animal edge)[23]. Instead,
124 proliferation is only detected in regions where undifferentiated cells with the typical morphology
125 of stem cells can be distinguished[23,24]. Thus, cycling somatic cells in *H. diminuta* would not include

126 differentiated cells, but would include stem cells and any dividing progeny. To label cycling cells,
127 we used two methods: (i) uptake of the thymidine analog F-*ara*-EdU[25] to mark cells in S-phase
128 and (ii) FISH to detect cell cycle-regulated transcripts, such as the replication licensing factor
129 *minichromosome maintenance complex component 2* (*mcm2*) and *histone h2b* (*h2b*), which are
130 conserved cycling-cell markers in free-living and parasitic flatworms[9,26]. We detected cycling
131 somatic cells throughout the tapeworm body (Fig. 2a-b). Contrary to previous results[23], we also
132 detected cycling cells in the head, though in small numbers (Fig. 2a). The scarcity of these cells
133 may be the reason they were originally missed. Taken together, cycling cells are present in all
134 regions, regardless of regeneration competence.

135 To further our understanding of how tapeworm stem cells are distributed and regulated, we
136 sought to identify stem cell markers. Stem cell genes have been discovered previously in flatworms
137 by identifying transcripts downregulated after exposure to irradiation, which depletes cycling
138 cells[9,26,27]. Exposing *H. diminuta* to 200 Gy x-irradiation reduced the number of cycling cells by
139 91±6% after 3 days (Fig. 2c-d) and abrogated both growth and regeneration (Fig. 2–figure
140 supplement 1a-b). This dosage is lethal; all fragments from worms exposed to 200 Gy x-irradiation
141 degenerated after 1 month (Fig. 2–figure supplement 1c-d). We leveraged the sensitivity of *H.*
142 *diminuta* to lethal irradiation in order to identify new molecular markers of cycling somatic cells
143 by RNA-seq (Fig. 2e). A *de novo* transcriptome of 14,346 transcripts was assembled (see Materials
144 and Methods) to which sequencing reads were mapped. We identified 683 transcripts that were
145 irradiation sensitive (downregulated; FDR ≤0.05) (Supplementary File 1a). Expression of
146 irradiation-sensitive transcripts by WISH was indeed reduced after exposure to irradiation,
147 validating our RNA-seq approach (Fig. 2–figure supplement 2).

148 Two rounds of expression screening were then applied to hone in on cycling-cell transcripts
149 from our irradiation-sensitive dataset (Fig. 2e). The position of cycling cells in the neck is spatially
150 restricted in a conserved pattern[28] (Fig. 3a): cycling cells reside in the neck parenchyma bounded
151 by the nerve cords and are absent from the animal edge where muscle and tegument are located[23].
152 Among 194 irradiation-sensitive transcripts that displayed clear WISH patterns, 63% were
153 expressed in the neck parenchyma, though in a variety of patterns (Fig. 3–figure supplement 1).
154 13% showed similar patterns to *h2b* and *mcm2* (Fig. 3b-c, Fig. 3–figure supplement 1b). These
155 include the predicted nucleic acid binding factors *Zn finger MYM type 3* (*zmym3)* and *pogo*
156 *transposable element with ZN finger domain-like* (*pogzl*), as well as *NAB co-repressor domain 2*
157 *superfamily member* (*nab2*) and nuclear lamina component *laminB receptor* (*lbr*). 25% of
158 irradiation-sensitive transcripts, were expressed in a minority of cells in the neck parenchyma (Fig.
159 3–figure supplement 1c). 24% were expressed within the parenchyma and more broadly toward
160 the animal edge (Fig. 3–figure supplement 1d). The remainder represented transcripts expressed
161 at segment boundaries or in differentiated tissues (Fig. 3–figure supplement 1e-f). All transcripts
162 that were expressed in the neck parenchyma were also found throughout the worm body, even in
163 the most posterior proglottids (Fig. 3–figure supplement 1b-c). In conclusion, irradiation-sensitive
164 transcripts identified by RNA-seq likely represent markers for stem cells, progenitors, and even
165 differentiated cells that were lost or compromised following irradiation.

166 To focus on transcripts with enriched expression in cycling cells, we performed double
167 FISH (dFISH) with irradiation-sensitive candidates and either *h2b* or *mcm2,* which we used
168 interchangeably as they are co-expressed in the neck parenchyma (Fig. 3–figure supplement 2).
169 After dFISH for 53 candidates, 72% of transcripts tested were co-expressed in cycling cells (Fig.
170 3–figure supplement 3a, Supplementary File 1b). The irradiation-sensitive transcripts from Fig. 3c

171 were indeed colocalized in cycling somatic cells (Fig. 3d). One transcript, the homeobox factor
172 *prospero* (*prox1*), was expressed exclusively in a subset of cycling cells (Fig. 3–figure supplement
173 3b). We confirmed that genes with expression that only partially overlapped in the neck
174 parenchyma, such as the Zn finger-containing gene *HDt_10981* and *palmitoyl-protein thioesterase*
175 *1 (ppt1)*, were expressed in both cycling cells and non-cycling cells (Fig. 3–figure supplement 3c).
176 We propose that these genes likely represent lineage-committed stem cells or progenitors for
177 tissues such as muscle, neurons, tegument, or protonephridia. 28% of irradiation-sensitive
178 transcripts were predominantly expressed in non-cycling cells that were juxtaposed to cycling cells
179 (Fig. 3–figure supplement 3d). The transcriptional heterogeneity detected in the cycling-cell
180 compartment is reminiscent of similar observations made in the regenerative planarian *S.*
181 *mediterranea*. A comparative analysis between verified tapeworm cycling-cell transcripts and their
182 putative planarian homologs revealed a number of transcripts with conserved expression in
183 cycling-cell populations from these distantly related flatworms (Supplementary File 1c) (see
184 Discussion). In summary, our analysis revealed a heterogeneous and complex mixture of cell types
185 or states in the neck parenchyma as well as within the cycling-cell population.

186 What role(s) do the newly identified cycling-cell genes play during regeneration? We
187 performed RNAi of target genes, confirmed knockdown by quantitative PCR (Fig. 4–figure
188 supplement 1), and assayed for defects in growth and regeneration (Fig. 4a). As a proof of
189 principle, we knocked down *h2b,* which should compromise growth due to cycling cell loss, as
190 observed in other flatworms[15,26]. Knockdown of *h2b, zmym3,* and *pogzl* each resulted in
191 diminished growth and regeneration (Fig. 4b-c). The number of proglottids regenerated was also
192 reduced, but could not be quantified as many RNAi worms were so thin and frail (Fig. 4b) that
193 proglottid definition was lost.

194 Are these RNAi-induced failures in growth and regeneration due to defects in the cycling-
195 cell population? RNAi knockdown of *h2b, zmym3,* and *pogzl* severely reduced the number of
196 proliferative cells in the neck that could incorporate F-*ara*-EdU (Fig. 4d-e). We also observed
197 fewer *mcm2*$^{+}$ cells after RNAi (Fig. 4f). Taken together, these results indicate that the cycling-cell
198 population is either lost or dysregulated. Therefore, *h2b, zmym3,* and *pogzl* are necessary for the
199 maintenance and/or proper function of cycling cells, likely including stem cells, in *H. diminuta*.
200 Although we have identified heterogeneity within the cycling-cell population of the neck
201 parenchyma and uncovered genes that are required for growth and regeneration, it remains unclear
202 why regeneration competence is restricted to the neck. By WISH and FISH, all cycling-cell
203 transcripts including *zmym3* and *pogzl* were detected throughout the whole tapeworm body (Fig.
204 4g, Fig. 3–figure supplement 1b-c). In the tapeworm posterior, *zmym3* and *pogzl* were expressed
205 in gonadal tissues (which contain mitotic germ cells) but also in somatic cells within the
206 parenchyma (Fig. 4–figure supplement 2). If *zmym3* and *pogzl* mark stem cells, this suggests that
207 stem cells reside even in posterior tissues that are not competent to regenerate. Since *zmym3* and
208 *pogzl* label all cycling cells, it is possible that stem cells of limited potential exist in the posterior,
209 but an elusive subpopulation of pluripotent stem cells is confined to the neck.
210 Since we observed an anterior bias in regenerative ability (Fig. 1h-i), we hypothesized that
211 RNA-seq may reveal an anteriorly biased stem cell distribution that may point us to a pluripotent
212 stem cell subpopulation. Thus, we performed RNA-seq of 1 mm anterior, middle, and posterior
213 neck fragments (Fig. 1h), and identified 461 anterior-enriched and 241 anterior-depleted
214 transcripts (Supplementary File 1d). By WISH, anterior-enriched and anterior-depleted transcripts
215 were often detected in corresponding gradients (Fig. 5a), but in patterns that were excluded from
216 the neck parenchyma. When we overlaid the anterior-enriched and -depleted datasets with our

217 irradiation-sensitive dataset, the majority of anterior-enriched transcripts (88%) were not
218 irradiation sensitive (Fig. 5b). Our results suggest that the A-P polarized signals across the neck
219 region arise predominantly within the non-cycling compartments.

220 Since our RNA-seq analysis identified 57 transcripts that were anterior enriched and
221 irradiation sensitive, we examined expression patterns within this category. We found 15
222 transcripts expressed in a subset of cells within the neck parenchyma (Fig. 5c) and initially
223 hypothesized that these transcripts may represent subsets of stem cells. We were able to
224 successfully test 8 candidates by dFISH with cycling-cell markers and found that the majority (7/8)
225 were not expressed in cycling cells (Fig. 5d, Supplementary File 1b). Only *prox1* was co-expressed
226 in cycling cells (Fig. 3–figure supplement 3b). At present, the identity and function of *prox1*$^{+}$ cells
227 is unknown. Furthermore, *prox1* is expressed throughout the tapeworm body (Figure 3 – figure
228 supplement 1). Thus, our analyses have not revealed an anteriorly biased subpopulation of stem
229 cells that confer regenerative ability.

230 With no evidence for a unique neck-specific subpopulation of stem cells, we hypothesized
231 that stem cells may be distributed throughout the tapeworm, but that extrinsic signals functioning
232 in the neck are necessary to instruct stem cell behavior and/or proglottid regeneration. We designed
233 a functional assay to test populations of cells for the ability to rescue regeneration, modelled after
234 similar experiments performed on planarians[8]. We exposed tapeworms to a lethal dose of x-
235 irradiation (200 Gy), injected cells from wild-type donors into the neck region, amputated 5 mm
236 anterior fragments, and assayed rescue of lethality and regeneration after 30 days *in vitro* (Fig. 6a).
237 Remarkably, bulk-cell transplants were able to either partially or fully rescue irradiated worms that
238 were destined to die (Fig. 6a, c). "Full" rescue was ascribed to worms with normal adult appearance
239 whereas "partial" rescue was assigned to cases in which proglottids were regenerated but the

240 worms displayed abnormalities, like contracted necks (Fig. 6–figure supplement 1a). We did not
241 observe any proglottid regeneration in irradiated worms with or without buffer injection (Fig. 6a,
242 c).

243 Is the rescue ability described above dependent on tapeworm cycling cells? We exposed
244 donors to F-*ara*-EdU for 1 hr, to label cycling cells prior to transplantation into irradiated hosts
245 (Fig. 6–figure supplement 1b). Though bulk-cell transplants were performed, injection sites
246 contained 0, 1, or small groups of F-ara-EdU$^+$ cells immediately after transplantations (Fig. 6–
247 figure supplement 1c), likely due to technical challenges. Despite this issue, we were able to detect
248 large colonies of F-ara-EdU$^+$ cells 3 days post-transplantation (Fig. 6–figure supplement 1d). We
249 also observed that some labeled cells were incorporated into terminally differentiated tissues at the
250 animal edge (Fig. 6–figure supplement 1d: inset). Thus, cycling cells from donors are able to
251 become established and differentiate inside the irradiated host.

252 To test if the cycling-cell population is necessary to rescue lethally irradiated tapeworms,
253 we depleted cycling cells from donor worms using 50 mM hydroxyurea (HU), which resulted in
254 96±3% loss of cycling cells after 6 days (Fig. 6–figure supplement 1e-f). Cycling cells are essential
255 for rescue of regeneration as injected cells from HU-treated donors rescued only 1% of the time,
256 compared to 26% rescue using cells sourced from sister donors that did not receive the drug (Fig.
257 6b-c). HU was used to deplete cycling cells instead of irradiation in order to avoid inducing DNA
258 damage in the transplanted cells. Cells transplanted from HU-treated donors had otherwise
259 comparable morphology to untreated cells (Fig. 6–figure supplement 1g). Our results suggest that
260 tapeworm cycling cells contain *bona fide* stem cell activity.

261 With this functional assay in hand, we examined the rescue ability of cells from anterior
262 donor tissues (including the regeneration-competent neck) compared to donor tissues from the

263 most posterior termini of 6 day-old tapeworms (which are regeneration incompetent and
264 exclusively comprised of proglottids). Cells from either region were able to rescue regeneration in
265 lethally irradiated tapeworms (Fig. 6b-c). Thus, cells from posterior proglottids were competent to
266 receive signals from the head and neck region that regulate regenerative ability. Interestingly, using
267 pulse-chase experiments with F-*ara*-EdU, we find that the cycling cells of posterior proglottids
268 can give rise to multiple differentiated cell types like muscle/tegument at the animal edge as well
269 as flame cells of the protonephridial system marked by anti-acetylated α-tubulin antibodies[17] (Fig.
270 6 - figure supplement 2). Thus, the cycling cells from tapeworm posteriors show hallmarks of stem
271 cell activity, despite the fact that this tissue is not competent to regenerate.

272 Taken together, the results of our study support the idea that the regeneration competence
273 of the neck is due to extrinsic signals that regulate regeneration, rather than intrinsic properties of
274 stem cells in the neck region (see Discussion). It appears that in tapeworms, location matters
275 enormously: the head and neck environment provide cues that regulate the ability of stem cells to
276 regenerate proglottids, even though cycling cells (and likely stem cells), are not anatomically
277 confined.

278 **Discussion**

279 Across the flatworm phylum, both free-living and parasitic worms maintain stem cells
280 throughout adulthood but display a range of regenerative abilities. The freshwater planarian *S.*
281 *mediterranea* can regenerate its whole body from tiny amputated fragments[6]. The blood fluke
282 *Schistosoma mansoni* cannot regenerate after amputation, though it does employ adult somatic
283 stem cells in other ways, such as to repair injury[29] and maintain its tegument[15,30]. Prior to this
284 study, the regenerative ability of tapeworms had never been tested comprehensively. Although it
285 was known that anterior fragments containing the head, neck, and immature proglottids could
286 regenerate into fully mature tapeworms once transplanted into a rat intestine[5,19], fragments lacking
287 heads could not be tested for regenerative ability using transplantation. Attempts were made to
288 suture *H. diminuta* fragments with mutilated or removed heads into a rat intestine but these
289 fragments were invariably flushed out[19]. Here we employ a robust *in vitro* culture system that
290 allowed us to test regeneration of any amputated *H. diminuta* fragment for the first time. We show
291 that the neck is both necessary and sufficient for proglottid regeneration, though this regenerative
292 ability is ultimately finite without regulatory signals that depend on the presence of the head. *H.*
293 *diminuta* is an intriguing model to discover signals that both drive and limit regenerative ability.

294 During homeostasis, the neck of *H. diminuta* serves as a "growth zone" from which
295 proglottids are thought to bud one at a time[31], thus, it makes intuitive sense that this tissue would
296 retain the ability to regenerate proglottids post-amputation. Furthermore, cells with the typical
297 morphology of stem cells reside in the neck[23]. However, we find that cycling cells are present in
298 all regions regardless of regenerative competence. Thus, it was necessary to embark on a more
299 thorough characterization of tapeworm cycling cells to understand how *H. diminuta* may regulate
300 stem cells and enable proglottid regeneration.

301 We depleted cycling cells in *H. diminuta* using irradiation and employed RNA-seq to
302 uncover potential stem cell regulators in an unbiased fashion. Though irradiation may have
303 secondary effects beyond stem cell depletion[26], this approach allowed us to generate an initial list
304 of candidate tapeworm stem cell genes. Using dFISH, we were able to verify 38 transcripts that
305 were expressed at least partially in cycling cells, providing the first molecular characterization of
306 this population in *H. diminuta*.

307 Adult somatic stem cells in free-living flatworms have already been well described
308 molecularly, and share many conserved regulators. However, parasitic flatworms have lost some
309 stem cell genes (e.g. *piwi*, *vasa*, and *tudor*)[32] but retained others (e.g. *argonaute*, *fgfr*)[9,10]. How do
310 the cycling-cell transcripts we identified in *H. diminuta* compare to stem cells in free-living
311 planarians?[33-36] (Supplementary File 1c). Of 38 verified tapeworm cycling-cell transcripts, 28 had
312 putative planarian homologs (tblasx E-value < 10^{-10}) though not all were reciprocal blast hits. 16
313 of these planarian transcripts were designated as cluster-defining genes in the Fincher et al. single-
314 cell sequencing dataset and 6/16 are neoblast cluster-defining genes. Plass et al. also performed
315 single-cell sequencing of planarians but most of the putative planarian homologs of tapeworm
316 cycling cell transcripts that we identified were not found in their dataset. However, 8/28 transcripts
317 showed enriched expression in neoblast clusters. We also compared the expression of these
318 planarian transcripts in RNA-seq of three cell populations sorted by fluorescence-activated cell
319 sorting (FACS): 1) X1 (neoblasts in G2/M), 2) X2 (G1 neoblasts and progenitors), and 3) Xins
320 (differentiated cells)[35,36]. We find that 22/28 putative planarian homologs of tapeworm cycling-
321 cell transcripts show enriched expression in either the X1 or X2 populations, which contain
322 neoblasts. Thus, despite >500 million years of separation between free-living and parasitic

323 flatworm evolution[37], tapeworm cycling-cell transcripts have conserved signatures with planarian
324 neoblasts.

325 In multiple species of flatworms, stem cells have been shown to be transcriptionally
326 heterogenous[26,33,38,39]. For example, in larvae of the tapeworm *Echinococcus multilocularis*, many
327 putative stem cell markers show limited overlapping gene expression patterns[10]. In keeping with
328 these findings, we observe transcriptional heterogeneity within the cycling-cell population of *H.*
329 *diminuta*. Additionally, we identified 23 transcripts, including *zmym3* and *pogzl*, that label all
330 cycling cells. Importantly, we were able to use RNAi to functionally verify that cycling-cell genes
331 like *zmym3* and *pogzl* are critical for stem cell maintenance and that inhibition of these genes leads
332 to impaired growth and regeneration. Both *zmym3* and *pogzl* are neoblast cluster-defining genes
333 in planarians (Supplementary File 1c) suggesting that their functions in stem cell regulation may
334 be conserved across the two species. In fact, the planarian homolog of tapeworm *pogzl*, *factor*
335 *initiating regeneration 1* (*fir1*), was recently shown to be expressed in planarian neoblasts[40]. RNAi
336 of *fir1* resulted in decreased cell division after amputation and failure to regenerate blastemas[40].
337 On the other hand, the function of *zmym3* in regeneration is not known, but in other systems,
338 *zmym3* regulates cell cycle progression[41] and DNA repair[42], two essential functions for stem cells.
339 Coincidently, both *zmym3* and *pogzl* are Zn finger proteins with predicted DNA-binding activity
340 and could function as transcriptional regulators of stem cells. Thus, it would be interesting to
341 further understand the mechanism of action of *zmym3* and *pogzl* in stem cells of parasitic and free-
342 living flatworms.

343 In this study, we showed the first use of RNAi in *H. diminuta*. RNAi has been demonstrated
344 previously in other tapeworm species[43-45], though it has not been widely adopted for studying
345 tapeworm biology due to technical challenges like poor knockdown efficacy, inefficient

346 penetrance, and the difficulty of *in vitro* culture. Taking advantage of the robust *in vitro* culture of
347 *H. diminuta*, our RNAi scheme can be expanded to ascertain functions for many parasitic flatworm
348 genes that thus far have been refractory to functional analyses.

349 Our screening strategy allowed us to verify genes with enriched expression in some or all
350 cycling cells; however, none of these genes were expressed exclusively in the neck. Since we had
351 observed that regenerative ability was anteriorly biased across the neck, we attempted to leverage
352 this observation and query whether a subpopulation of pluripotent cycling cells may be
353 asymmetrically distributed across the neck and would be identifiable by RNA-seq. Through A-P
354 transcriptional profiling of the neck, we identified 461 anterior-enriched transcripts, but the vast
355 majority of them were neither irradiation-sensitive nor detected in cycling cells by dFISH. Thus,
356 a subpopulation of neck-resident pluripotent stem cells, seems unlikely to explain the region-
357 specific regenerative ability of tapeworms. Nonetheless, our study does not exclude the existence
358 of a subpopulation of pluripotent stem cells that may be stably maintained in the adult. Future
359 studies using single-cell RNA sequencing are likely to provide a thorough characterization of adult
360 somatic stem cells in *H. diminuta*, as has been the case for planarians[33,34,39].

361 Is the neck competent to regenerate because of a unique stem cell population that has yet
362 to be identified, or because of signals extrinsic to stem cells that make the neck permissive for
363 regeneration? Tapeworms exposed to a lethal dose of irradiation prior to amputation are not
364 competent to regenerate and will eventually degenerate and die. However, transplantation of cells
365 from wild-type donors into the necks of irradiated tapeworms rescued lethality and regeneration.
366 This rescue ability is severely compromised if donor worms are first depleted of cycling cells using
367 drug treatment with HU, suggesting that some or all cycling cells have stem cell ability.
368 Interestingly, stem cell ability is not restricted to cells from regeneration-competent regions: cells

369 from posterior tissues that do not regenerate proglottids are still able to rescue regeneration when
370 transplanted into the neck. These data strongly suggest that the microenvironment within the neck
371 confers regenerative ability to this region.

372 The interplay between intrinsic and extrinsic stem cell regulatory signals has been shown
373 to play important roles in regeneration. Head regeneration was induced in three naturally
374 regeneration-deficient planarian species by manipulating the gradient of Wnt signaling by RNAi[46-
375 48]. These planarians maintain pluripotent stem cells but do not normally regenerate heads from
376 posterior tissues due to inappropriately high levels of Wnt signaling, which inhibit anterior
377 regeneration. As in planarians, gradients of Wnt signaling delineate A-P polarity in tapeworms[49].
378 Our transcriptional profiling of the neck A-P axis has already revealed hundreds of candidate genes
379 with polarized expression profiles. Future experiments will help clarify how Wnt signaling and
380 other A-P axis regulation in the neck impacts tapeworm regeneration.

381 Several plausible models can explain region-specific regeneration in *H. diminuta*. Head-
382 dependent signals may create gradients across the neck that inhibit proglottidization and are
383 necessary to maintain the neck as an unsegmented tissue. Proglottids can only form once the
384 inhibitory signals are sufficiently diminished (Fig. 6d). In this model, the neck is competent to
385 regenerate because of its juxtaposition to the head. After decapitation, the head-dependent signals
386 eventually dissipate and segmentation signals dominate at the expense of the neck. The cellular
387 source of the head-dependent signals and their molecular identity will be exciting avenues for
388 future research.

389 In addition to its function in maintaining the neck, the head may also play a role in stem
390 cell regulation (Fig. 6e). The head may regulate a niche (directly or indirectly) that is necessary
391 for the maintenance of pluripotency in the neck. In this model, stem cells are collectively

392 pluripotent only when they receive head-dependent niche signals, thus limiting regenerative
393 potential to the neck. Alternatively, stem cells may depend on a local niche that is independent of
394 the head. In this model, stem cells have the capacity to form all cell lineages from any amputated
395 fragment; however, the extrinsic signals that activate proglottid formation are restricted to the
396 posterior neck region. Identifying the stem cell niche and its relationship to the head and neck
397 microenvironment will provide crucial insights into our understanding of tapeworm regeneration.
398

399 **Conclusion**

400 Our study shows that *H. diminuta* is a powerful developmental model for understanding
401 intrinsic and extrinsic regulation of stem cells and regeneration. The regionally limited
402 regenerative biology of *H. diminuta* and the technical advances put forth in this work show that
403 we can exploit this tapeworm to understand the complexities of stem cell regulation in parasites.
404 We defined heterogenous stem cells that are collectively pluripotent but that require extrinsic head-
405 dependent signals to enable persistent proglottid regeneration. Understanding how the stem cell
406 niche we describe is regulated may have broad implications for elucidating stem cell biology in
407 parasitic flatworms, as well as other regenerative animals.
408

409 **Acknowledgements**

410 We thank: members of the Newmark lab, especially Melanie Issigonis and Umair Khan,
411 for discussions and comments on the manuscript; Alvaro Hernandez (Roy J. Carver Biotechnology
412 Center, University of Illinois at Urbana-Champaign) for RNA-seq; and Bret Duffin (Morgridge
413 Institute for Research) for invaluable assistance with irradiation. This work was supported by NIH
414 R21AI119960. PAN is an investigator of the Howard Hughes Medical Institute.

415 **Materials and Methods**

416 Animal care and use

417 Infective *H. diminuta* cysts were obtained from Carolina Biological (132232). To obtain
418 adult tapeworms, 100-400 cysts were fed to Sprague-Dawley rats by oral gavage in ~0.5 mL of
419 0.85% NaCl. Rats were euthanized in a CO_2 chamber 6 days post-gavage, tapeworms were flushed
420 out of the small intestine, and washed in 1X Hanks Balanced Salt Solution (HBSS; Corning) (140
421 mg/L $CaCl_2$, 100 mg/L $MgCl_2.6H_2O$, 100 mg/L $MgSO_4.7H_2O$, 400 mg/L KCl, 60 mg/L KH_2PO_4,
422 350 mg/L $NaHCO_3$, 8 g/L NaCl, 48 mg/L Na_2HPO_4, 1 g/L D-glucose, no phenol red). Rodent care
423 was in accordance with protocols approved by the Institutional Animal Care and Use Committee
424 (IACUC) of the University of Wisconsin-Madison (M005573).

425 *In vitro* parasite culture

426 Biphasic parasite cultures were prepared based on the Schiller method[18]. Briefly, the solid
427 phase was made in 50 mL Erlenmeyer flasks by mixing 30% heat-inactivated defibrinated sheep
428 blood (Hemostat) with 70% agar base for 10 mL blood-agar mixture per flask. Fresh blood was
429 heat-inactivated at 56°C for 30 min then kept at 4°C and used repeatedly for one week by first
430 warming the blood to 37°C. The agar base was prepared from 8 g Difco nutrient agar and 1.75 g
431 NaCl in 350 mL water, autoclaved, and stored at 4°C. Before use, the agar base was microwaved
432 to liquify, and cooled to below 56°C before mixing with warmed blood. After the blood-agar
433 mixture solidified, 10 mL of Working Hanks 4 (WH4; 1X HBSS/4 g/L total glucose/1X antibiotic-
434 antimycotic (Sigma)) was added. Each flask was topped with a gas-permeable stopper (Jaece
435 Identi-plug) and pre-incubated at 37°C in hypoxia (3% CO_2/5% O_2/92% N_2) overnight before use.
436 Before tapeworms were transferred into the flasks, the liquid phase was adjusted to pH7.5 with
437 200 μL 7.5% $NaHCO_3$ (Corning). Tapeworms were first washed in WH4 for 10 mins at 37°C in

438 petri dishes pre-coated with 0.5% BSA to inhibit sticking. Transfers to pre-cultured flasks were
439 performed by gently lifting the worms with a stainless-steel hook (Moody Tools) and immersing
440 them in the liquid phase. Tapeworms were grown in hypoxia and transferred to fresh cultures every
441 3-4 days.

442 Fixation and DAPI Staining

443 Tapeworms were heat-killed by swirling in 75°C water for a few seconds until the worms
444 relaxed and elongated, then fixative (4% formaldehyde in Phosphate Buffered Saline with 0.3%
445 TritonX-100 (PBSTx)) was added immediately for 30 min-2hr at room temperature or overnight
446 at 4°C. For DAPI staining, samples were incubated in 1 μg/mL DAPI (Sigma) in PBSTx overnight
447 at 4°C and cleared in 80% glycerol/10 mM Tris pH7.5/1 mM EDTA overnight at room temperature
448 before mounting.

449 F-*ara*-EdU[31] uptake and staining

450 For F-*ara*-EdU pulse, tapeworms were incubated in 0.1 μM F-*ara*-EdU (Sigma) in 1%
451 DMSO at 37°C in WH4. Tapeworms were heat-killed (above) and fixed in 4% formaldehyde/10%
452 DMSO/1% NP40/PBSTx. Large tissues/worms were permeabilized by incubating in PBSTx at
453 room temp for several days. Additional permeabilization was achieved by treatment with 10
454 μg/mL Proteinase-K/0.1% SDS/PBSTx for 10-30 min at room temperature, fixed in 4%
455 formaldehyde/PBSTx for 10 min before samples were cut into small pieces or retained whole in
456 PBSTx. Samples were further permeabilized in PBSTx/10% DMSO/1% NP40 for 20min-1 hr
457 (depending on size) before performing the click-it reaction[50] with Oregon Green 488 azide
458 (Invitrogen). Signal was detected using anti-Oregon Green 488-HRP antibody (1:1000;
459 Invitrogen) in K-block (5% Horse serum/0.45% fish gelatin/0.3% Triton-X/0.05% Tween-
460 20/PBS) [51] followed by 10-20 min Tyramide Signal Amplification (TSA) reaction [52]. Tiled

461 confocal z-stacks through the anterior of the worms were taken and cell numbers were counted
462 using background subtraction on Imaris software. F-*ara*-EdU^{+} cells were normalized to worm area
463 from maximum projections of the DAPI stain. Flame cells were stained using an anti-acetylated
464 α-tubulin mouse antibody at 1:500 (sc-23950, Santa Cruz) as described previously[17].

465 Irradiation

466 Most irradiation was performed using a CellRad irradiator (Faxitron Bioptics) at 200 Gy
467 (150 kV, 5 mA) with two exceptions. Due to instrument failure, a cesium irradiator was used for
468 one rescue experiment with donors +/- HU (Fig. 6b) at 400 Gy (92±5 % cycling cell loss 3 days
469 post-irradiation). The rescue experiment with +/- HU donors was performed a third time once we
470 gained access to an x-irradiator (Xstrahl RS225 Cell Irradiator), where the lethal dose was 200 Gy
471 (63±10 % cycling cell loss 3 days post-irradiation). All three experiments gave similar results
472 despite the use of different irradiators. In all cases, lethal irradiation was determined as the dosage
473 at which tapeworms degenerated, had 0 proglottids, and were inviable after 30 days in culture.
474 Irradiation was performed in WH4 in BSA-coated petri dishes.

475 Transcriptome assembly

476 RNA was collected from five regions: 1) head and neck, 2) immature proglottids, 3) mature
477 reproductive proglottids, 4) gravid proglottids, and 5) mixed larval stages isolated from beetles.
478 The first three regions covered the entirety of 3.5-week old adult tapeworms. Gravid proglottids
479 were taken from posteriors of 10-week old tapeworms. Paired-end libraries were constructed with
480 2 x 150 bp reads from a HiSeq2500 chip. 2 x ~30 million reads were obtained for each sample.
481 The transcriptome was assembled from three components: 1) map-based assembly, 2) *de novo*
482 assembly, and 3) Maker predictions from Wormbase Parasite. The map-based assembly was
483 performed using TopHat2 with the 2014 *H. diminuta* draft genome courtesy of Matt Berriman

484 (Wellcome Sanger Institute, UK). 15,859 transcripts were assembled using TopHat. *De novo*
485 assembly was performed using Velvet/Oases and resulted in 144,682 transcripts. There were
486 11,275 predicted Maker transcripts and 73.2% matched (>95% along the length) to the TopHat
487 transcripts. The remaining predicted transcripts that were not represented in the TopHat dataset
488 were added for a combined TopHat/predicted set of 17,651 transcripts. Most of the Oases
489 transcripts matched to the TopHat/predicted set but 35,300 or 24.4% of the Oases transcripts did
490 not (>75% match cut-off). These transcripts could be transcripts missed in the genome,
491 transcription noise, non-coding transcripts, or contamination. We found significant contamination
492 from beetle tissue in the larval tapeworm sample (more below). Initial filtering for contamination
493 excluded 1,388 transcripts (from beetle, rat, bacterial, and viral sources). At this point 51,563
494 transcripts were retained from the three methodologies described above and were processed for
495 further filtering.

496 There was significant contamination from beetle tissues that had adhered to the tapeworm
497 larvae, which produced transcripts with best hits to beetle proteins (*Ixodes scapularis,*
498 *Harpegnathos saltator, Monodelphis domestica, Nasonia vitripennis, Pediculus humanus*
499 *corporis, Solenopsis invicta, Tenebrio molitor,* or *Tribolium castaneum*). Most of the transcripts
500 were from the Oases *de novo* assembly and did not match the *H. diminuta* genome. Furthermore,
501 they were strongly over-represented in the larval sample only. To filter out beetle contamination,
502 we removed 11,918 transcripts from the Oases assembly without matches to the *H. diminuta*
503 genome that showed >90% expression (by RPKM) in the larval sample.

504 To the remaining 39,645 transcripts, we applied additional filters: 1) Remove transcripts if
505 average RPKM<1 unless the transcript is long (>1000 bp), has a long ORF (>500 bp) or is
506 annotated. 11,615 transcripts were removed as they met none of these criteria. 2) A stringent

507 expression cut-off was applied to the remaining Oases transcripts; transcripts were discarded if
508 average RPKM<5 and maximum RPKM<10 unless the transcripts were long (>1000 bp), had long
509 ORFs (>500 bp) or were annotated. 8,027 transcripts were removed. 3) 51 transcripts were
510 removed because they are mitochondrial or rRNAs. 4) An ORF size filter was applied to remove
511 all transcripts with ORF <300 bp unless they are annotated. 5,331 transcripts were removed. 5)
512 For the Maker predicted transcripts, expression and size filters were applied to remove transcripts
513 with expression <1 RPKM and size <500 bp. 275 transcripts were removed.

514 Our final transcriptome is comprised of 14,346 transcripts (84.9% TopHat, 8.4% Maker
515 predictions, 6.1% Oases with match to genome, and 0.6% Oases without match to genome). The
516 total transcriptome size is 34 Mb with average transcript length of 2,354 bp. This Transcriptome
517 Shotgun Assembly project has been deposited at DDB/ENA/Genbank under the accession
518 GHNR00000000. The version described in this paper is the first version, GHNR01000000. All
519 sequence reads are available at GenBank Bioproject PRJNA546290.

520 RNA-seq for differential gene expression analyses

521 Tissue was collected and immediately frozen on dry ice in 100 μL Trizol (Life
522 Technologies) before RNA extraction. Tissue homogenization was performed as the mixture was
523 in a semi-frozen state using RNase-free pestles and a pestle motor. RNA was purified using the
524 Direct-zol RNA MiniPrep kit (Zymo). RNA quality was assessed using Bioanalyzer, libraries were
525 prepared with TruSeq Stranded mRNAseq Sample Prep kit (Illumina), and sequenced on two lanes
526 on a HiSeq2500 chip. We performed paired-end sequencing and obtained ~20 million reads per
527 sample. Samples were obtained in triplicate. To identify irradiation-sensitive transcripts, 2 mm
528 anterior tapeworm fragments were cut from 10 worms after 3 days *in vitro*. To identify
529 differentially expressed transcripts across the neck A-P axis, 1 mm fragments were cut from 20

530 freshly obtained 6 day-old tapeworms. Paired-end reads were mapped to the transcriptome (above)
531 using default settings on CLC Genomics Workbench 6 (Qiagen) except that read alignments were
532 done with a relaxed length fraction of 0.5. Differential gene expression analysis was done with the
533 same software using estimate tagwise dispersions on total read counts and a total count filter cut-
534 off of 5 reads. All sequence reads used for differential genes expression analyses are available at
535 GenBank Bioproject PRJNA546293.

536 Cloning

537 Target genes were amplified using PCR with Platinum Taq (Life Technologies) from
538 cDNA generated from RNAs extracted from tapeworm anteriors to enrich for neck transcripts.
539 PCR products were inserted via TA-mediated cloning into the previously described vector
540 pJC53.2[53] pre-digested with *Eam11051*. Anti-sense riboprobes could be generated by *in vitro*
541 transcription with SP6 or T3 RNA polymerases. For RNAi, dsRNA was generated using T7 RNA
542 polymerase. For sequences and primers, refer to Supplementary File 1e.

543 *In situ* hybridization

544 WISH and FISH protocols were modified from previously published methods for
545 planarians[52] and the mouse bile-duct tapeworm *Hymenolepis microstoma* [54]. Tapeworms were heat
546 killed and fixed in 4% formaldehyde/10% DMSO/1% NP40/PBSTx for 30 min at room
547 temperature before washing and dehydration into methanol. Dehydrated samples were frozen at -
548 30°C for at least 2 days. After rehydration, samples were permeabilized in 10 μg/mL Proteinase-
549 K/0.1% SDS/PBSTx for 30 min, washed into 0.1 M Triethanolamine pH7-8 (TEA), 2.5 μL/mL
550 acetic anhydride was added for 5 min with vigorous swirling, acetic anhydride step was repeated,
551 washed in PBSTx, and post-fixed in 4% formaldehyde/PBSTx for 10 min. Probe synthesis,
552 hybridization, and staining were performed as previously described[52] using probe concentrations

553 at ~50 ng/mL for 16-48 hrs at 56°C. All probes were synthesized with either DIG or DNP haptens
554 and detected using the following antibodies, all at 1:2000: anti-DIG-AP (Sigma), anti-DIG-POD
555 (Sigma), anti-DNP-HRP (Vector Labs). Colorimetric development was done using NBT
556 (Roche)/BCIP (Sigma) or with Fast-Blue (Sigma)[55]. Fluorescent signal was visualized after 10-20
557 min TSA reaction[52]. DAPI staining and mounting were performed as described above.

558 Imaging

559 Confocal imaging was performed on a Zeiss LSM 880 with the following objectives:
560 20X/0.8 NA Plan-APOCHROMAT, 40X/1.3 NA Plan-APOCHROMAT, and 63X/1.4 NA Plan-
561 APOCHROMAT. WISH samples and whole-mount DAPI-stained worms were imaged using
562 Zeiss AxioZoom V16 macroscope. Image processing was performed using ImageJ for general
563 brightness/contrast adjustments, maximum-intensity projections, and tile stitching[56].

564 RNAi

565 dsRNA was synthesized as previously described[57] and resuspended at concentrations ~ 1.5-
566 2 μg/μL. For control injections, 1.5 kb dsRNA derived from *ccdB* and *camR*-containing insert of
567 the pJC53.2 vector was used[53]. 6 day-old tapeworms were obtained and microinjected with dsRNA
568 using femtotips II via the Femtojet injection system (Eppendorf) to obtain spreading across the
569 first ~ 3-4 mm anterior of the tapeworm. The spread of injected fluids could be detected by a
570 temporary increase in opacity. 500 hPa injection pressure for 0.3-1 s was used per injection site.
571 Whole tapeworms were cultured *in vitro* for 3 days, 2 mm anterior fragments were amputated,
572 worms were re-injected with dsRNA on day 6, and cultured *in vitro* for an additional 9 days before
573 termination.

574 qPCR for target gene knockdown efficacy

575 Whole worms (6 days old) were injected with dsRNA throughout and frozen in Trizol on
576 dry ice after 6 days *in vitro* for RNA extraction according to manufacturer's protocol and DNAse
577 (Promega) treatment for 30 min at 37°C. cDNA synthesis was performed using SuperScriptIII
578 First-Strand Synthesis System (Invitrogen) with Oligo$(dT)_{20}$ primers followed by iScript cDNA
579 Synthesis Kit (Bio-Rad). qPCR was performed using GoTaq Mastermix (Promega) on a
580 StepOnePlus real-time PCR machine (Applied Biosystems). *60S ribosomal protein L13*
581 (*60Srpl13)* was used as an internal normalization control. For primers refer to Supplementary File
582 1e.

583 Hydroxyurea (HU) treatment

584 Tapeworms were treated with HU (Sigma) or HBSS (for controls) every day for a total of
585 6 days. HU stock solution was made fresh every day at 2 M in HBSS. 250 μL was added to each
586 flask of tapeworms for final concentration of 50 mM. HU is unstable at 37°C so worms were
587 transferred into fresh HU-containing media every two days, and fresh HU was added every other
588 day.

589 Cell transplantations

590 For dissociated cell preparations, tapeworms were placed in a drop of calcium-magnesium
591 free HBSS (CMF HBSS, Gibco), minced into small pieces with a tungsten needle, incubated in
592 3X Trypsin-EDTA (Sigma) in CMF HBSS for 30 min at 37°C and dissociated using a dounce
593 homogenizer (Kontes). Cells were pelleted by centrifugation at 250 g for 5 min. The cell pellet
594 was washed in CMF HBSS and passed through cell strainers at 100 μm, 40 μm, 20 μm, and 10
595 μm (Falcon and Sysmex) with one spin and wash in between. Cells were pelleted and resuspended
596 in 200-400 μL WH4 with 0.05% BSA. Cell injections were performed using the Cell Tram Oil 4
597 injection system (Eppendorf) into the necks of irradiated worms. For +/- HU donors, cell

598 concentrations were measured using a hemocytometer and normalized (to ~10^8 cells/mL) to ensure
599 equal numbers of cells were injected. For all rescue experiments, cells were injected into irradiated
600 hosts on the same day that the hosts were irradiated. After 3 days *in vitro,* 5 mm anterior fragments
601 were amputated and grown for an additional 27 days.

602 Statistical Analysis.

603 Statistical analyses were performed using Prism7 software (GraphPad Prism). All
604 experiments were repeated at least twice. All measurements were taken from distinct samples.
605 Error bars, statistical tests, number of replicates (N) and sample sizes (n) are indicated in
606 corresponding figure legends. Either Dunnett's or Tukey's multiple comparison tests were used
607 for one-way ANOVAs. SD=standard deviation. P-values: ns= not significant, *= $p \leq 0.5$, ****=
608 $p \leq 0.0001$.

609

610 **References**

611 1. Del Brutto, O. H. Human cysticercosis (*Taenia solium*). *Trop Parasitol* **3,** 100–103
612 (2013).
613 2. Craig, P. & Ito, A. Intestinal cestodes. *Curr. Opin. Infect. Dis.* **20,** 524–532 (2007).
614 3. Roberts, L. S. Development of *Hymenolepis diminuta* in its definitive host in *Biology of*
615 *the Tapeworm Hymenolepis diminuta.* 357–423 (Academic Press, Inc., NY, 1980).
616 4. Arai, H. P. (Ed.) *Biology of the Tapeworm Hymenolepis diminuta*. (Academic Press, Inc.,
617 NY, 1980).
618 5. Read, C. P. Longevity of the tapeworm, *Hymenolepis diminuta*. *J. Parasitol.* **53,** 1055–
619 1056 (1967).
620 6. Newmark, P. A. & Sánchez Alvarado, A. Not Your Father's Planarian: A Classic Model
621 Enters The Era Of Functional Genomics. *Nat. Rev. Genet.* **3,** 210–219 (2002).
622 7. Reddien, P. W. The Cellular and Molecular Basis for Planarian Regeneration. *Cell* **175,**
623 327–345 (2018).
624 8. Baguñà, J. The planarian neoblast: the rambling history of its origin and some current
625 black boxes. *Int. J. Dev. Biol.* **56,** 19–37 (2012).
626 9. Collins, J., III *et al.* Adult somatic stem cells in the human parasite *Schistosoma mansoni*.
627 *Nature* **494,** 476–479 (2013).
628 10. Koziol, U., Rauschendorfer, T., Zanon Rodríguez, L., Krohne, G. & Brehm, K. The
629 unique stem cell system of the immortal larva of the human parasite *Echinococcus*
630 *multilocularis*. *EvoDevo* **5,** 10 (2014).
631 11. Koziol, U. *et al.* A Novel Terminal-Repeat Retrotransposon in Miniature (TRIM) Is
632 Massively Expressed in *Echinococcus multilocularis* Stem Cells. *Genome Biol Evol* **7,**
633 2136–2153 (2015).
634 12. Wang, B., Collins, J., III & Newmark, P. A. Functional genomic characterization of
635 neoblast-like stem cells in larval *Schistosoma mansoni*. *Elife* **2,** e00768 (2013).
636 13. Koziol, U., Domínguez, M. F., Marín, M., Kun, A. & Castillo, E. Stem cell proliferation
637 during in vitro development of the model cestode *Mesocestoides corti* from larva to adult
638 worm. *Front. Zool.* **7,** 22 (2010).
639 14. Collins, J., III. Platyhelminthes. *Current Biology* **27,** R252–R256 (2017).
640 15. Collins, J., III, Wendt, G. R., Iyer, H. & Newmark, P. A. Stem cell progeny contribute to
641 the schistosome host-parasite interface. *Elife* **5,** 243 (2016).
642 16. Brehm, K. & Koziol, U. On the importance of targeting parasite stem cells in anti-
643 echinococcosis drug development. *Parasite* **21,** 72 (2014).
644 17. Rozario, T. & Newmark, P. A. A confocal microscopy-based atlas of tissue architecture in
645 the tapeworm *Hymenolepis diminuta*. *Exp. Parasitol.* **158,** 31–41 (2015).
646 18. Schiller, E. L. A simplified method for the in vitro cultivation of the rat tapeworm,
647 *Hymenolepis diminuta*. *J. Parasitol.* **51,** 516–518 (1965).
648 19. Goodchild, C. G. Transfaunation and Repair of Damage in the Rat Tapeworm,
649 *Hymenolepis diminuta*. *J. Parasitol.* **44,** 345–351 (1958).
650 20. Baguñà, J., Salo, E. & Auladell, C. Regeneration and Pattern-Formation in Planarians .3.
651 Evidence That Neoblasts Are Totipotent Stem-Cells and the Source of Blastema Cells.
652 *Development* **107,** 77–86 (1989).
653 21. Newmark, P. A. & Sánchez Alvarado, A. Bromodeoxyuridine Specifically Labels the
654 Regenerative Stem Cells of Planarians. *Dev. Biol.* **220,** 142–153 (2000).

655 22. Ladurner, P., Rieger, R. & Baguñà, J. Spatial distribution and differentiation potential of
656 stem cells in hatchlings and adults in the marine platyhelminth macrostomum sp.: a
657 bromodeoxyuridine analysis. *Dev. Biol.* **226,** 231–241 (2000).
658 23. Bolla, R. I. & Roberts, L. S. Developmental physiology of cestodes. IX. Cytological
659 characteristics of the germinative region of *Hymenolepis diminuta*. *J. Parasitol.* **57,** 267–
660 277 (1971).
661 24. Sulgostowska, T. The development of organ systems in cestodes. I. A study of histology
662 of *Hymenolepis diminuta* (Rudolphi, 1819)(Hymenolepididae). *Acta Parasitologica*
663 *Polonica* **20,** 449–462 (1972).
664 25. Neef, A. B. & Luedtke, N. W. Dynamic metabolic labeling of DNA in vivo with
665 arabinosyl nucleosides. *Proceedings of the National Academy of Sciences* **108,** 20404–
666 20409 (2011).
667 26. Solana, J. *et al.* Defining the molecular profile of planarian pluripotent stem cells using a
668 combinatorial RNAseq, RNA interference and irradiation approach. *Genome Biol.* **13,** R19
669 (2012).
670 27. Eisenhoffer, G. T., Kang, H. & Sánchez Alvarado, A. Molecular Analysis of Stem Cells
671 and Their Descendants during Cell Turnover and Regeneration in the Planarian *Schmidtea*
672 *mediterranea*. *Cell Stem Cell* **3,** 327–339 (2008).
673 28. Koziol, U. & Castillo, E. Cell proliferation and differentiation in cestodes. *Research in*
674 *Helminths* 121–138 (2011).
675 29. Collins, J. N. R. & Collins, J., III. Tissue Degeneration following Loss of *Schistosoma*
676 *mansoni* cbp1 Is Associated with Increased Stem Cell Proliferation and Parasite Death In
677 Vivo. *PLoS Pathog* **12,** e1005963 (2016).
678 30. Wendt, G. R. *et al.* Flatworm-specific transcriptional regulators promote the specification
679 of tegumental progenitors in *Schistosoma mansoni*. *Elife* **7,** (2018).
680 31. Lumsden, R. D. & Specian, R. The morphology, histology, and fine structure of the adult
681 stage of the cyclophyllidean tapeworm *Hymenolepis diminuta* in *Biology of the Tapeworm*
682 *Hymenolepis diminuta.* 157–280 (Academic Press., Inc, NY, 1980).
683 32. Tsai, I. J. *et al.* The genomes of four tapeworm species reveal adaptations to parasitism.
684 *Nature* **496,** 57–63 (2013).
685 33. Fincher, C. T., Wurtzel, O., de Hoog, T., Kravarik, K. M. & Reddien, P. W. Cell type
686 transcriptome atlas for the planarian *Schmidtea mediterranea*. *Science* **360,** eaaq1736
687 (2018).
688 34. Plass, M. *et al.* Cell type atlas and lineage tree of a whole complex animal by single-cell
689 transcriptomics. *Science* **360,** eaaq1723 (2018).
690 35. Labbé, R. M. *et al.* A comparative transcriptomic analysis reveals conserved features of
691 stem cell pluripotency in planarians and mammals. *Stem Cells* **30,** 1734–1745 (2012).
692 36. Rozanski, A. *et al.* PlanMine 3.0-improvements to a mineable resource of flatworm
693 biology and biodiversity. *Nucleic Acids Res.* **47,** D812–D820 (2019).
694 37. Laumer, C. E., Hejnol, A. & Giribet, G. Nuclear genomic signals of the
695 'microturbellarian' roots of platyhelminth evolutionary innovation. *Elife* **4,** e05503 (2015).
696 38. van Wolfswinkel, J. C., Wagner, D. E. & Reddien, P. W. Single-Cell Analysis Reveals
697 Functionally Distinct Classes within the Planarian Stem Cell Compartment. *Cell Stem Cell*
698 **15,** 326–339 (2014).
699 39. Zeng, A. *et al.* Prospectively Isolated Tetraspanin+ Neoblasts Are Adult Pluripotent Stem
700 Cells Underlying Planaria Regeneration. *Cell* **173,** 1593–1608.e20 (2018).

701 40. Han, X.-S. *et al.* Neoblast-enriched zinc finger protein FIR1 triggers local proliferation
702 during planarian regeneration. *Protein Cell* **10,** e1004400 (2018).
703 41. Hu, X. *et al.* Gene knockout of *Zmym3* in mice arrests spermatogenesis at meiotic
704 metaphase with defects in spindle assembly checkpoint. *Cell Death Dis* **8,** e2910 (2017).
705 42. Leung, J. W. C. *et al.* ZMYM3 regulates BRCA1 localization at damaged chromatin to
706 promote DNA repair. *Genes Dev.* **31,** 260–274 (2017).
707 43. Pierson, L. *et al.* RNA interference in a cestode reveals specific silencing of selected
708 highly expressed gene transcripts. *Int. J. Parasitol.* **40,** 605–615 (2010).
709 44. Mizukami, C. *et al.* Gene silencing in *Echinococcus multilocularis* protoscoleces using
710 RNA interference. *Parasitol. Int.* **59,** 647–652 (2010).
711 45. Spiliotis, M. *et al. Echinococcus multilocularis* primary cells: improved isolation, small-
712 scale cultivation and RNA interference. *Mol. Biochem. Parasitol.* **174,** 83–87 (2010).
713 46. Sikes, J. M. & Newmark, P. A. Restoration of anterior regeneration in a planarian with
714 limited regenerative ability. *Nature* **500,** 77–80 (2013).
715 47. Liu, S. Y. *et al.* Reactivating head regrowth in a regeneration-deficient planarian species.
716 *Nature* **500,** 81–84 (2013).
717 48. Umesono, Y. *et al.* The molecular logic for planarian regeneration along the anterior-
718 posterior axis. *Nature* **500,** 73–76 (2013).
719 49. Koziol, U., Jarero, F., Olson, P. D. & Brehm, K. Comparative analysis of Wnt expression
720 identifies a highly conserved developmental transition in flatworms. *BMC Biol.* **14,** 1
721 (2016).
722 50. Salic, A. & Mitchison, T. J. A chemical method for fast and sensitive detection of DNA
723 synthesis in vivo. *Proceedings of the National Academy of Sciences* **105,** 2415–2420
724 (2008).
725 51. Collins, J., III, King, R. S., Cogswell, A., Williams, D. L. & Newmark, P. A. An atlas for
726 *Schistosoma mansoni* organs and life-cycle stages using cell type-specific markers and
727 confocal microscopy. *PLoS Negl Trop Dis* **5,** e1009 (2011).
728 52. King, R. S. & Newmark, P. A. In situ hybridization protocol for enhanced detection of
729 gene expression in the planarian *Schmidtea mediterranea*. *BMC Dev. Biol.* **13,** 8 (2013).
730 53. Collins, J., III *et al.* Genome-wide analyses reveal a role for peptide hormones in planarian
731 germline development. *PLoS Biol.* **8,** e1000509 (2010).
732 54. Olson, P. D. *et al.* Genome-wide transcriptome profiling and spatial expression analyses
733 identify signals and switches of development in tapeworms. *EvoDevo* **9,** R991 (2018).
734 55. Currie, K. W. *et al.* HOX gene complement and expression in the planarian *Schmidtea*
735 *mediterranea*. *EvoDevo* **7,** 7 (2016).
736 56. Preibisch, S., Saalfeld, S. & Tomancak, P. Globally optimal stitching of tiled 3D
737 microscopic image acquisitions. *Bioinformatics* **25,** 1463–1465 (2009).
738 57. Rouhana, L. *et al.* RNA interference by feeding in vitro-synthesized double-stranded RNA
739 to planarians: methodology and dynamics. *Dev. Dyn.* **242,** 718–730 (2013).
740

741 **Figure Legends**

742

743 **Figure 1. Regeneration competence of *H. diminuta*. a**, Schematic of *H. diminuta* adults. **b**,
744 DAPI-stained 1 cm fragments grown *in vitro*. **c-d**, Quantification of proglottid number and growth
745 in length from (**b**). Error bars=SD, N=2-5, n=7-21; one-way ANOVA with Dunnett's multiple
746 comparison test, compared to day 0. **e**, Representative DAPI-stained "neck only" fragment
747 regeneration. **f-g**, 2 mm anterior fragments, with or without the head, grown *in vitro* for 12-15 days
748 and then re-amputated serially. Error bars=SD, +head: one-way ANOVA with Tukey's multiple
749 comparison test, -head: Student's t-test. **h-i**, DAPI-stained 1 mm fragments from the anterior,
750 middle, and posterior of the neck grown *in vitro*. Error bars=SD, N=3, n=22-29, one-way ANOVA
751 with Tukey's multiple comparison test.

752

753 **Figure 2. Cycling somatic cells are distributed throughout the tapeworm body and are**
754 **irradiation sensitive. a-b,** Maximum-intensity projections of confocal sections showing
755 distribution of cycling cells by 2 hr uptake of F-*ara*-EdU (**a**) or FISH for *mcm2* (**b**). Fewer cycling
756 cells were found in the head (box), while abundant cycling cells were observed in both somatic
757 and gonadal tissues throughout the body. t=testis, o=ovary. **c**, Maximum-intensity projections of
758 tile-stitched confocal sections after 1 hr uptake of F-*ara*-EdU (green) 3 days post-irradiation. **d**,
759 Quantification of F-*ara*-EdU$^+$ cell inhibition from (**c**). Error bars=SD, N=2, n=11 and 9, Student's
760 t-test. **e**, RNA-seq strategy to identify genes expressed in cycling cells. (Nuclei are counterstained
761 with DAPI (gray) in this and all subsequent figures.)

762

763

764 **Figure 3. Expression screening for cycling cell markers. a**, Confocal section of a tapeworm
765 anterior. Cycling cells (*mcm2*: magenta) in the neck parenchyma are between the nerve cords
766 (*cadherin*: green). s: sucker, nc: nerve cord, oc: osmoregulatory canal, t: tegument, m: muscle, and
767 p: parenchyma. **b**, WISH of known cycling-cell markers *h2b* and *mcm2*. sc: scolex (head) and n:
768 neck. **c**, WISH for irradiation-sensitive transcripts expressed in the neck parenchyma. **d**, Confocal
769 sections of dFISH for irradiation-sensitive transcripts (green) with *h2b* or *mcm2* (magenta) from
770 neck parenchyma. Cyan arrowheads indicate cells magnified at the far right.
771
772 **Figure 4. RNAi to identify genes required for growth and regeneration in *H. diminuta*. a**,
773 Schematic of RNAi paradigm. **b**, DAPI-stained worms after RNAi knockdown of *h2b, zmym3*,
774 and *pogzl*. **c**, Quantification of worm lengths after RNAi. Error bars=SD, N=3-4, n=26-37, one-
775 way ANOVA with Dunnett's multiple comparison test compared to control. **d-e**, Maximum-
776 intensity projections (**d**) and quantification (**e**) of cycling-cell inhibition after 1 hr F-*ara*-EdU
777 uptake following RNAi. Worms with degenerated necks were excluded from analysis. Error
778 bars=SD, N=3, n=11-14, one-way ANOVA with Dunnett's multiple comparison test compared to
779 control. **f**, *mcm2* WISH on worm anteriors after RNAi. **g**, WISH of *zmym3* and *pogzl* sampled from
780 anterior to posterior of adult 6 day-old worms. ga: genital anlagen; t: testis; o: ovary.
781
782 **Figure 5. RNA-seq identifies anterior-enriched transcripts that are expressed predominantly**
783 **in non-cycling cells. a**, WISH of tapeworm anteriors for transcripts that were anterior-enriched
784 (FC ≥1.5, FDR ≤0.05) or -depleted (FC ≤-1.5, FDR ≤0.05) by RNA-seq. Panels oriented anterior
785 facing left. **b,** Differential gene expression analyses of 1 mm anterior, middle, and posterior neck
786 fragments overlaid with irradiation-sensitive transcripts. **c**, WISH of transcripts that were anterior-

787 enriched and irradiation-sensitive by RNA-seq that showed expression in a subset of cells in the
788 neck parenchyma. **d**, Confocal sections from dFISH of anterior-enriched transcripts (green) and
789 *mcm2* (magenta). Cyan arrowheads indicate cells that are magnified at the far right.
790
791 **Figure 6. Stem cell activity depends on cycling cells but is not confined to cells from the neck.**
792 **a-b**, DAPI-stained worms after rescue with cell transplantations from whole-worm donors (**a**) or
793 sourced from depicted donors (**b**). **c**, Quantification of rescue phenotypes from pooled
794 experiments. Number of animals listed above bars. **d**, Model for head-dependent neck maintenance
795 and proglottid formation. **e**, Models of head-dependent or -independent stem cell niches.
796
797 **Figure 1–figure supplement 1. Phenotypic description of regeneration-incompetent tissues of**
798 ***H. diminuta*.** **a**, Quantification of mean proglottid length (fragment length/# of proglottids). Mean
799 proglottid length from body only fragments are significantly longer than mean proglottid length
800 from either head+neck+body or neck+body fragments. Error bars=SD, N=2-5, n=7-21; one-way
801 ANOVA with Tukey's multiple comparison test done at each timepoint. **b**, Confocal sections of
802 the most mature proglottids from "body only" fragments showing immature proglottids at day 0
803 and a gravid proglottid at day 9. t: testis, ga: genital anlagen, and u: uterus. **c**, Micrographs of
804 amputated heads over 30 days *in vitro* showing a failure to regenerate. White arrowheads point to
805 examples shown in the insets.
806
807 **Figure 1–figure supplement 2. Unsegmented neck is depleted after decapitation.** DAPI-
808 stained worms with or without decapitation were cultured *in vitro* for the indicated number of days.

809 Red arrowheads mark the position of the first visible proglottid. After 18 days *in vitro,* the neck
810 tissue is no longer identifiable in -head worms.
811
812 **Figure 2–figure supplement 1. Irradiation inhibits tapeworm regeneration. a**, DAPI staining
813 of 5 mm anterior fragments from control and irradiated worms before and after 6 days *in vitro*
814 culture. **b**, Quantification of (**a**). Error bars=SD, N=2, n= 10-16, one-way ANOVA with Tukey's
815 multiple comparison test. **c-d**, Lethal dose of irradiation was revealed when 5 mm anterior
816 fragments were amputated and grown *in vitro* for 1 month from worms exposed to 0 Gy or 200 Gy
817 x-irradiation. The irradiated samples in (**d**) are shown to scale as an inset in (**c**).
818
819 **Figure 2–figure supplement 2. Validation of RNA-seq by WISH after irradiation.** WISH (with
820 Fast-Blue Development) from two regions of the tapeworm: anterior (left) and body (right), 3 days
821 post-irradiation.
822
823 **Figure 3–figure supplement 1. WISH patterns of irradiation-sensitive transcripts identified**
824 **using RNA-seq. a**, Classification of WISH expression patterns of irradiation-sensitive transcripts.
825 **b-f**, Examples of transcripts expressed in the neck parenchyma (**b**), in subsets of cells within the
826 neck (**c**), in neck parenchyma and broadly toward the animal edge where differentiated muscle and
827 tegument are located (**d**), at segment boundaries (**e**), and in differentiated tissues (**f**) like the
828 osmoregulatory canals (left) and nervous system (right).
829

830 **Figure 3–figure supplement 2. Colocalization of *mcm2* and *h2b*.** Confocal section of dFISH to
831 detect *mcm2* (green) and *h2b* (magenta) in the neck parenchyma at low (top) and high (bottom)
832 magnification.
833
834 **Figure 3–figure supplement 3. The cycling somatic cell population is heterogeneous. a**,
835 Summary of different co-expression patterns obtained from 53 dFISH experiments. Also refer to
836 Supplementary File 1b. **b-d**, Confocal sections of dFISH to detect irradiation-sensitive transcripts
837 (green) with *h2b* or *mcm2* (magenta). Cyan arrowheads indicate cells magnified at the far right.
838 For (**c**), yellow arrowheads point to examples of expression in non-cycling cells.
839
840 **Figure 4–figure supplement 1. Validation of target gene knockdown by quantitative PCR.**
841 Knockdown of *h2b*, *zmym3*, or *pogzl* in whole worms observed after RNAi. Error bars: RQ
842 min/max, N=2, n=3 each.
843
844 **Figure 4–figure supplement 2. Expression of *zmym3* and *pogzl* in posterior proglottids.**
845 Confocal sections of *in situ* hybridizations showing expression of cycling-cell transcripts in the
846 gonads as well as in the non-gonadal parenchyma. t: testis and o: ovary.
847
848 **Figure 6–figure supplement 1. Stem cell activity depends on cycling cells. a**, DAPI-stained
849 worms showing phenotypes observed after attempted rescue of irradiation-induced lethality. No
850 rescue results in degenerated worms with no proglottids, full rescue results in normal worms with
851 multiple proglottids, and partial rescue refers to worms with visible proglottids but with defects
852 such as contracted necks. **b**, Schematic for rescue experiment using donors with labeled cycling

853 cells. **c-d**, Maximum-intensity projections of tile-stitched confocal sections 0 or 3 days post-
854 transplanation according to (**b**). Injections sites marked with asterisks. White arrowhead points to
855 a single transplanted cell. After 3 days, large colonies of F-*ara*-EdU$^+$ (green) cells could be
856 detected with some labeled cells incorporated into terminally differentiated tissues at the animal
857 edge (inset). **e**, Maximum-intensity projections of tile-stitched confocal sections after 1 hr F-*ara*-
858 EdU uptake (green) from control worms or worms cultured with hydroxyurea (HU) for 6 days. **f**,
859 Quantification of cycling cells from (**e**). Error bars=SD, N=3, n=11 and 8, Student's t-test. **g**, Cell
860 morphology with or without HU treatment prior to transplantation.
861
862 **Figure 6–figure supplement 2. Cycling cells give rise to multiple lineages in both anterior and**
863 **posterior fragments. a**, Schematic of F-*ara*-EdU pulse-chase protocol to label cycling cells from
864 2 mm amputated fragments and detect their progeny after 3 days. **b-c**, Confocal sections of both
865 anterior and posterior fragments on day 0 showing the absence of F-*ara*-EdU (green) at the animal
866 edge (yellow double-headed arrows) where differentiated muscle and tegument are located. After
867 3 days, F-*ara*-EdU has chased into the edge-most nuclei (examples marked by red arrowheads).
868 **d-f**, Confocal sections from posterior fragments after F-*ara*-EdU pulse-chase in combination with
869 acetylated α-tubulin antibody staining to label flame cells (magenta). Yellow arrowheads point to
870 F-*ara*-EdU$^-$ flame cell nuclei at day 0 (**d**) which are exclusively post-mitotic. Cyan arrowheads
871 point to two examples of flame cell nuclei that are F-*ara*-EdU$^+$ after 3 days chase (**e-f**).

872 Supplementary File 1a**. Irradiation-sensitive transcripts identified by RNA-seq.**

873

874 Supplementary File 1b**. Summary of dFISH experiments with irradiation-sensitive transcripts**

875 **and cycling cell markers *h2b* and/or *mcm2*.**

876

877 Supplementary File 1c**. Comparative analysis of verified tapeworm cycling-cell transcripts to**

878 **gene expression datasets for planarian neoblasts.**

879

880 Supplementary File 1d**. Anterior-enriched and anterior-depleted neck transcripts by RNA-**

881 **seq.**

882

883 Supplementary File 1e**. Sequences and primers for all genes reported.**

884

Figure 1

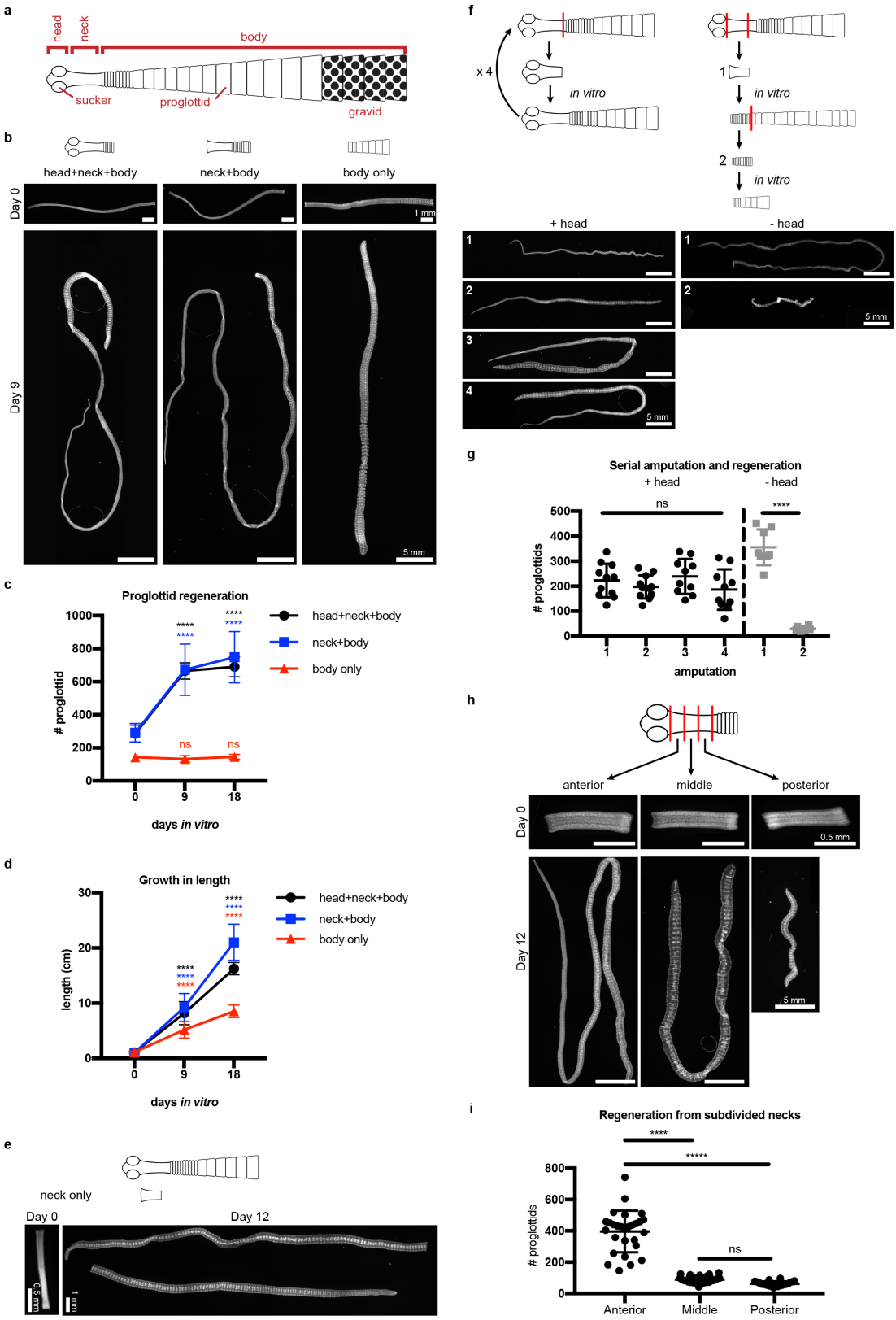
a
head
neck
body
sucker
proglottid
gravid
b
head+neck+body
neck+body
body only
Day 0
Day 9
1 mm
5 mm
c
Proglottid regeneration
proglottid
days in vitro
head+neck+body
neck+body
body only
ns
d
Growth in length
length (cm)
days in vitro
head+neck+body
neck+body
body only
e
neck only
Day 0
Day 12
0.5 mm
1 mm
f
x 4
in vitro
1
2
+ head
- head
5 mm
g
Serial amputation and regeneration
+ head
- head
proglottids
amputation
ns
h
anterior
middle
posterior
Day 0
Day 12
0.5 mm
5 mm
i
Regeneration from subdivided necks
proglottids
Anterior
Middle
Posterior
ns

Figure 2

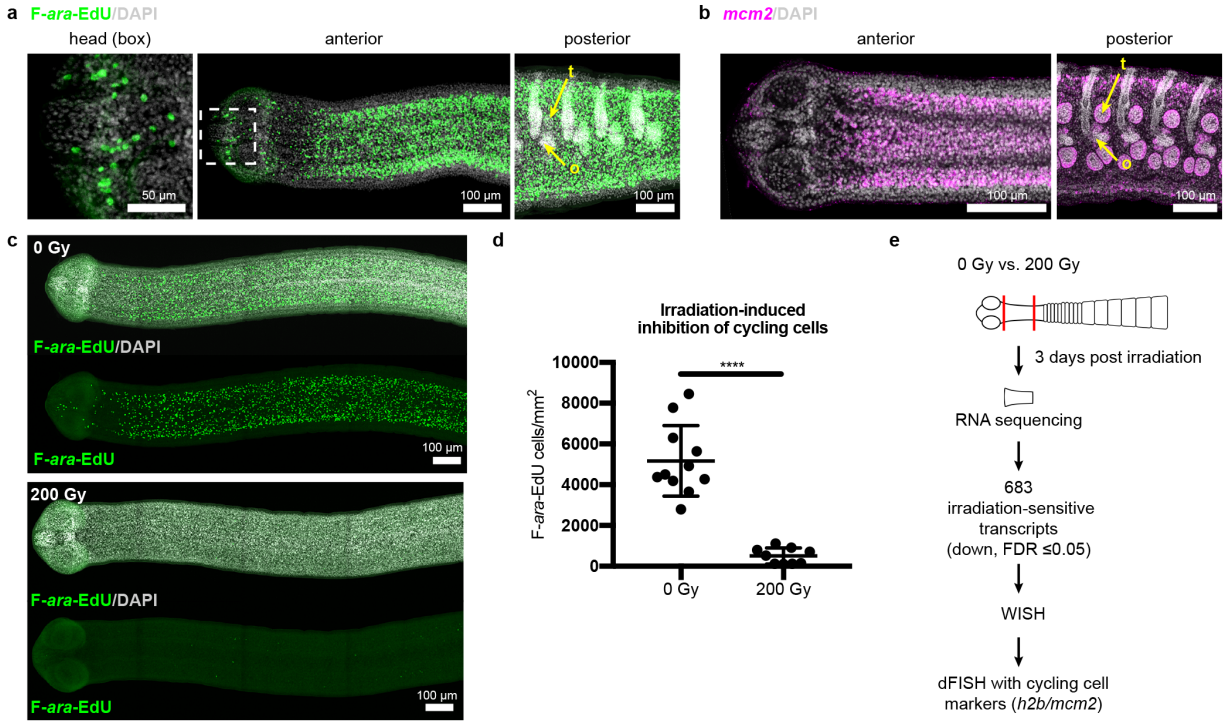
a
F-ara-EdU/DAPI
head (box)
anterior
posterior
t
o
50 µm
100 µm
100 µm
b
mcm2/DAPI
anterior
posterior
t
o
100 µm
100 µm
c
0 Gy
F-ara-EdU/DAPI
F-ara-EdU
100 µm
200 Gy
F-ara-EdU/DAPI
F-ara-EdU
100 µm
d
Irradiation-induced
inhibition of cycling cells
****
F-ara-EdU cells/mm2
10000
8000
6000
4000
2000
0
0 Gy
200 Gy
e
0 Gy vs. 200 Gy
3 days post irradiation
RNA sequencing
683
irradiation-sensitive
transcripts
(down, FDR ≤0.05)
WISH
dFISH with cycling cell
markers (h2b/mcm2)

Figure 3

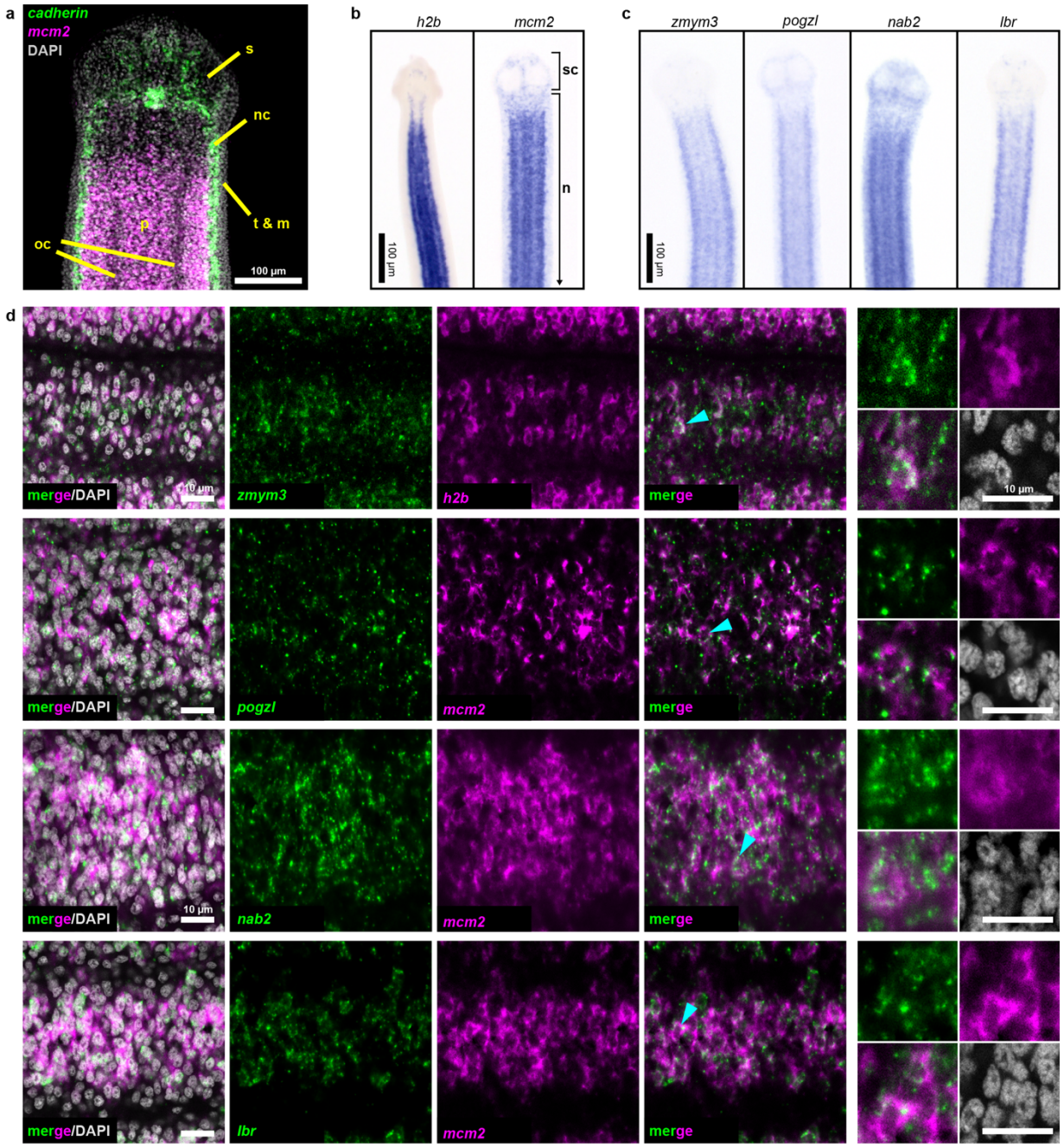
a
cadherin
mcm2
DAPI
s
nc
t & m
oc
100 µm
b
h2b
mcm2
sc
n
100 µm
c
zmym3
pogzl
nab2
lbr
100 µm
d
merge/DAPI
10 µm
zmym3
h2b
merge
10 µm
merge/DAPI
pogzl
mcm2
merge
merge/DAPI
10 µm
nab2
mcm2
merge
merge/DAPI
lbr
mcm2
merge

Figure 4

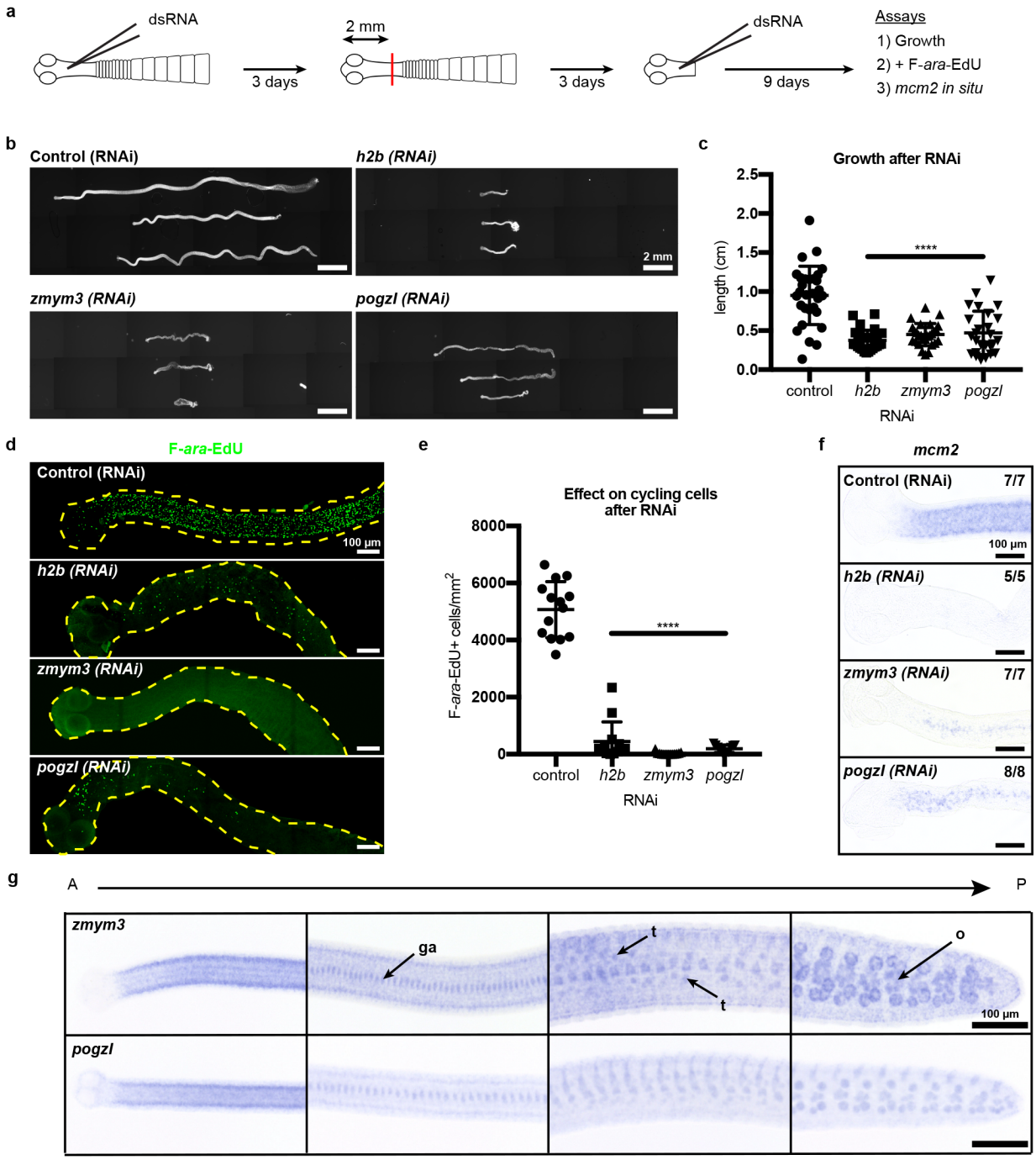
a
dsRNA
3 days
2 mm
3 days
dsRNA
9 days
Assays
1) Growth
2) + F-ara-EdU
3) mcm2 in situ
b
Control (RNAi)
h2b (RNAi)
2 mm
zmym3 (RNAi)
pogzl (RNAi)
c
Growth after RNAi
length (cm)
2.5
2.0
1.5
1.0
0.5
0.0
****
control
h2b
zmym3
pogzl
RNAi
d
F-ara-EdU
Control (RNAi)
100 µm
h2b (RNAi)
zmym3 (RNAi)
pogzl (RNAi)
e
Effect on cycling cells after RNAi
F-ara-EdU+ cells/mm2
8000
6000
4000
2000
0
****
control
h2b
zmym3
pogzl
RNAi
f
mcm2
Control (RNAi) 7/7
100 µm
h2b (RNAi) 5/5
zmym3 (RNAi) 7/7
pogzl (RNAi) 8/8
g
A
P
zmym3
ga
t
t
o
100 µm
pogzl

Figure 5

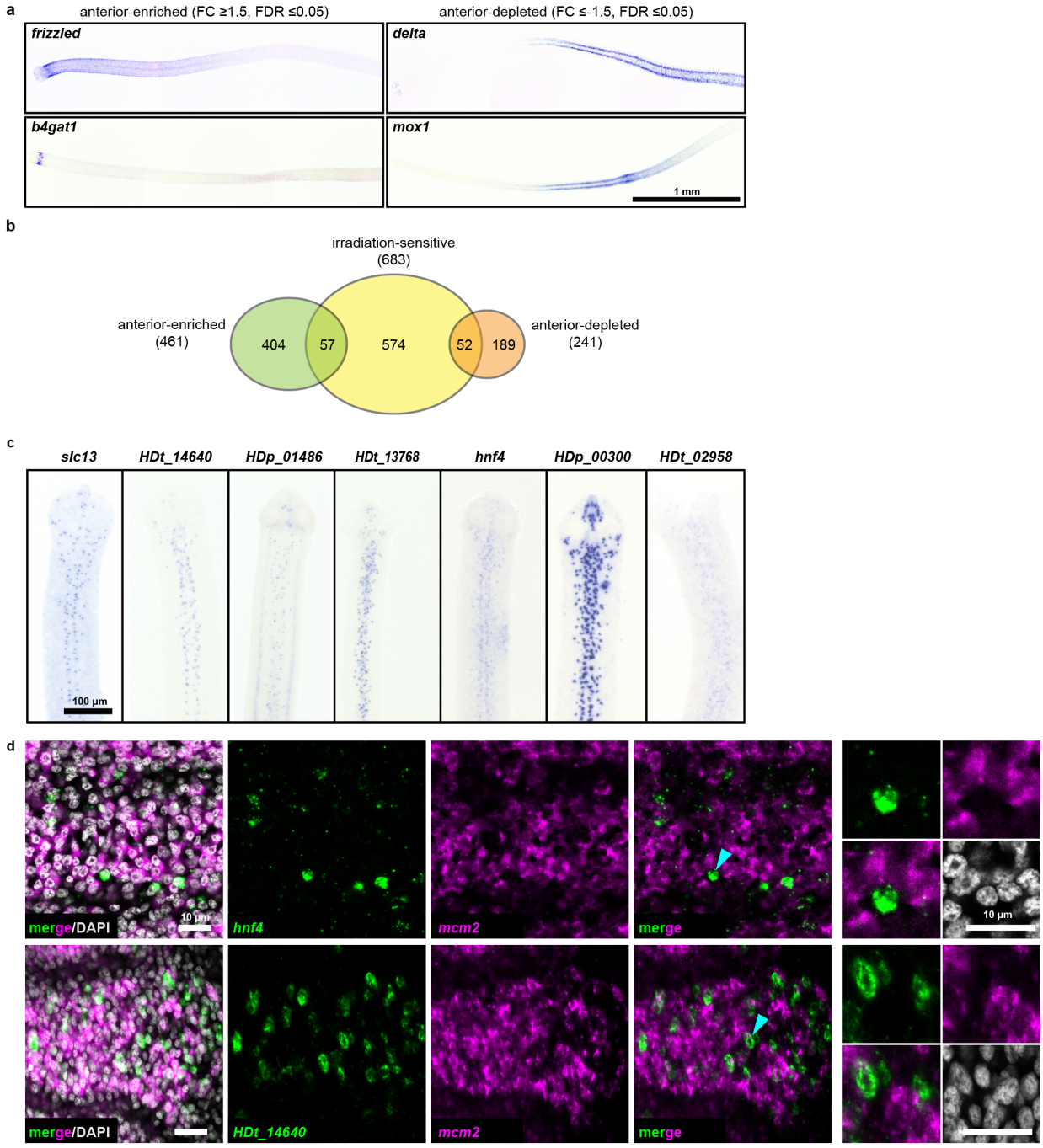
a
anterior-enriched (FC ≥1.5, FDR ≤0.05)
anterior-depleted (FC ≤-1.5, FDR ≤0.05)
frizzled
delta
b4gat1
mox1
1 mm
b
irradiation-sensitive
(683)
anterior-enriched
(461)
404
57
574
52
189
anterior-depleted
(241)
c
slc13
HDt_14640
HDp_01486
HDt_13768
hnf4
HDp_00300
HDt_02958
100 µm
d
merge/DAPI
10 µm
hnf4
mcm2
merge
10 µm
merge/DAPI
HDt_14640
mcm2
merge

Figure 6

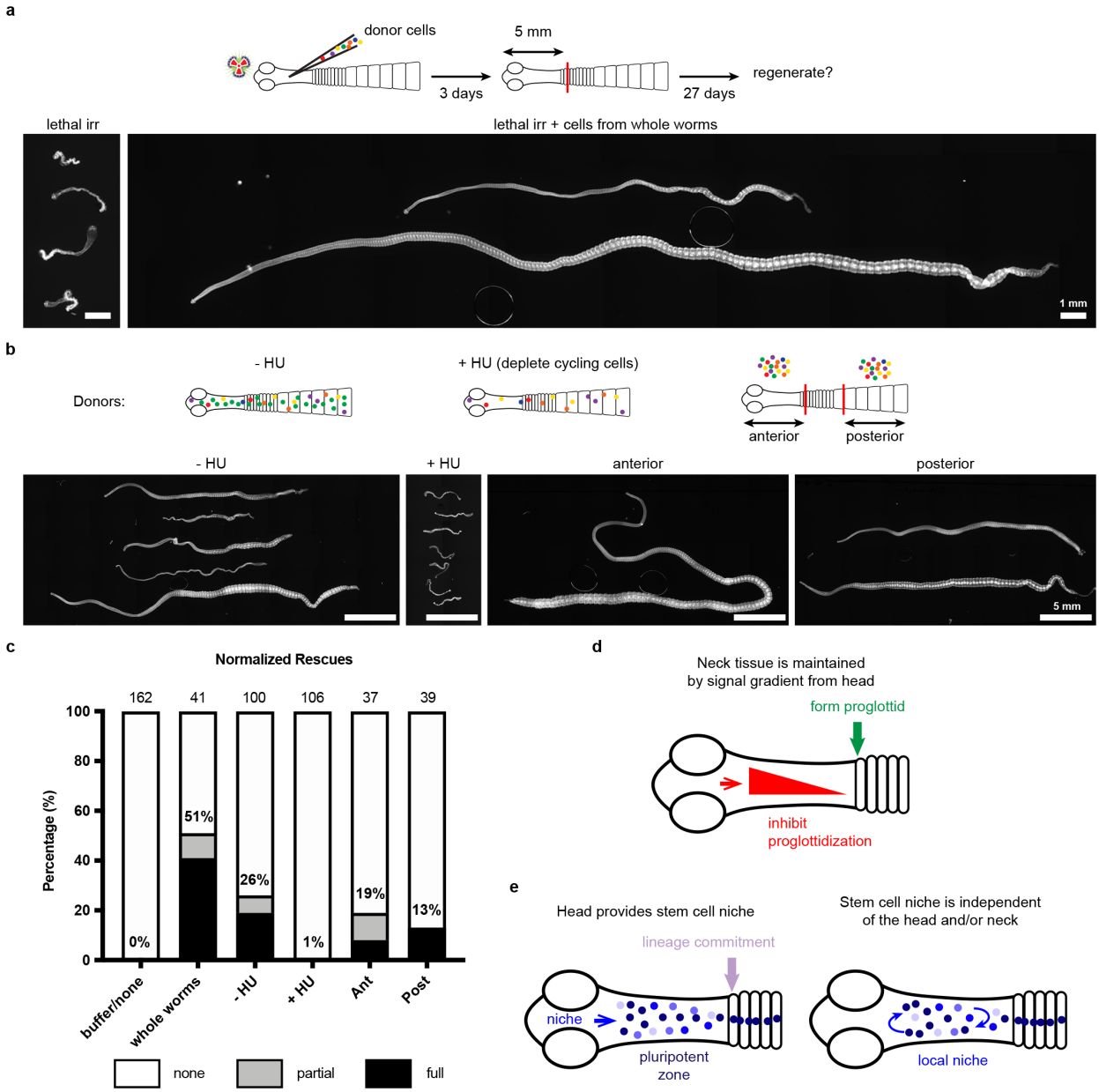
a
donor cells
5 mm
3 days
27 days
regenerate?
lethal irr
lethal irr + cells from whole worms
1 mm
b
Donors:
- HU
+ HU (deplete cycling cells)
anterior
posterior
- HU
+ HU
anterior
posterior
5 mm
c
Normalized Rescues
Percentage (%)
162
41
100
106
37
39
0%
51%
26%
1%
19%
13%
buffer/none
whole worms
- HU
+ HU
Ant
Post
none
partial
full
d
Neck tissue is maintained
by signal gradient from head
form proglottid
inhibit
proglottidization
e
Head provides stem cell niche
lineage commitment
niche
pluripotent
zone
Stem cell niche is independent
of the head and/or neck
local niche

Figure 1 – figure supplement 1

a

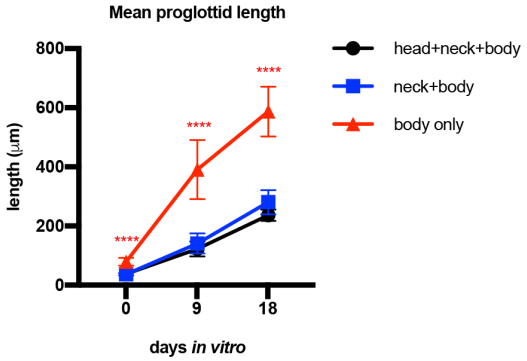

b

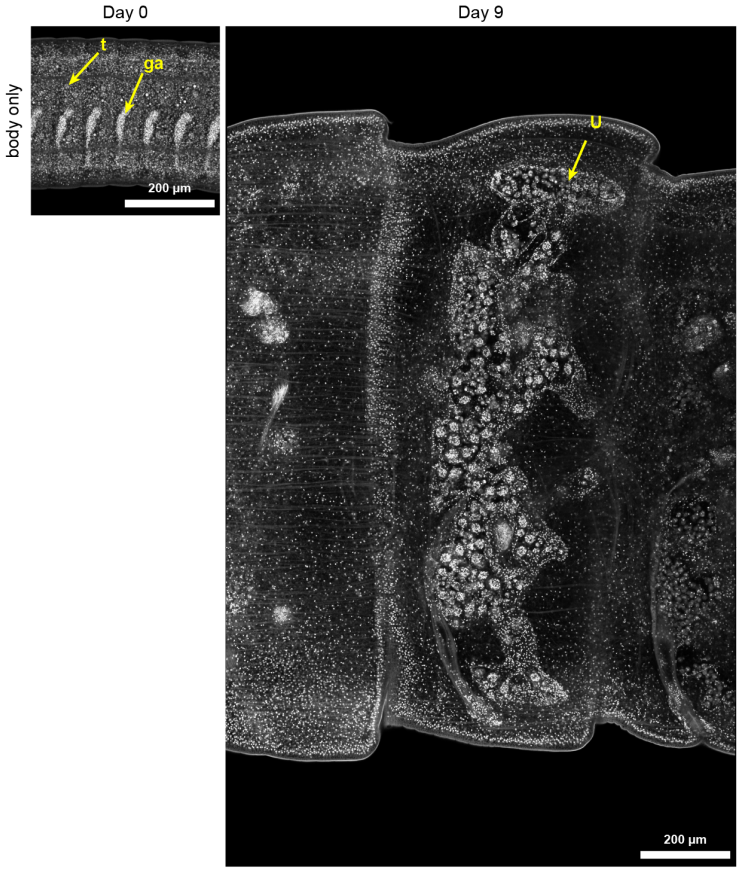

c

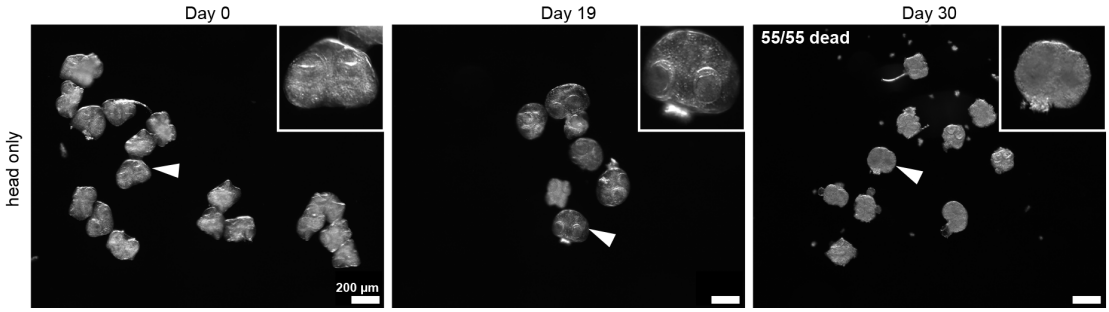

Figure 1 – figure supplement 2

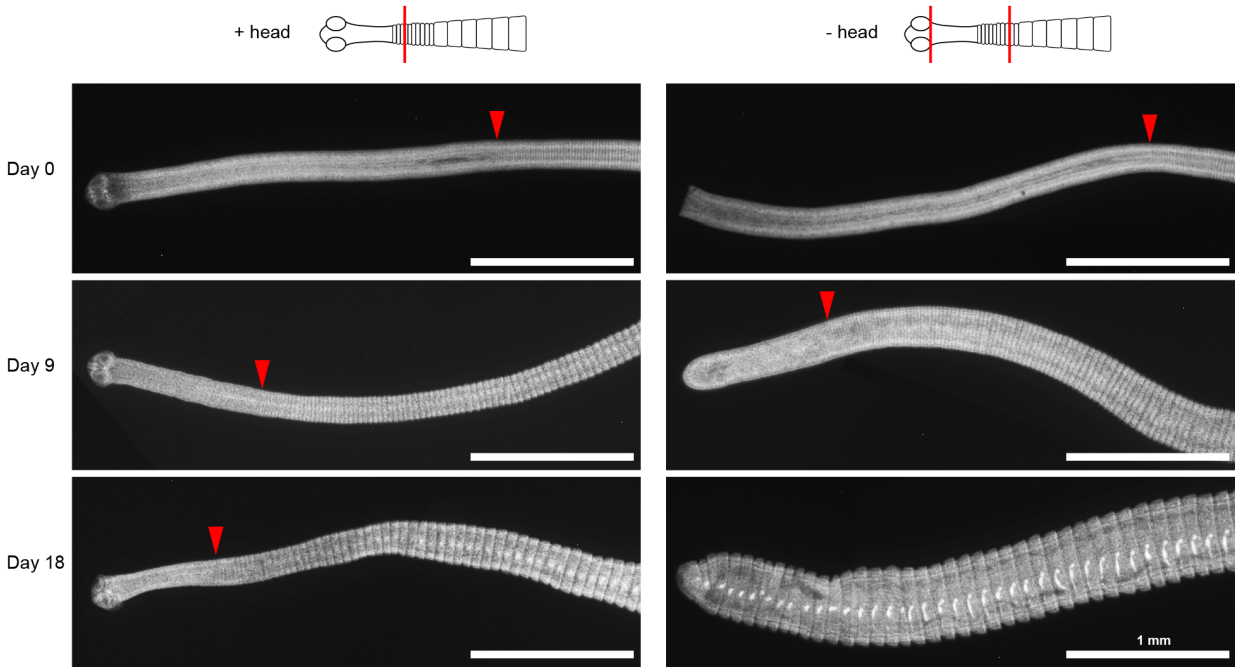

Figure 2 – figure supplement 1

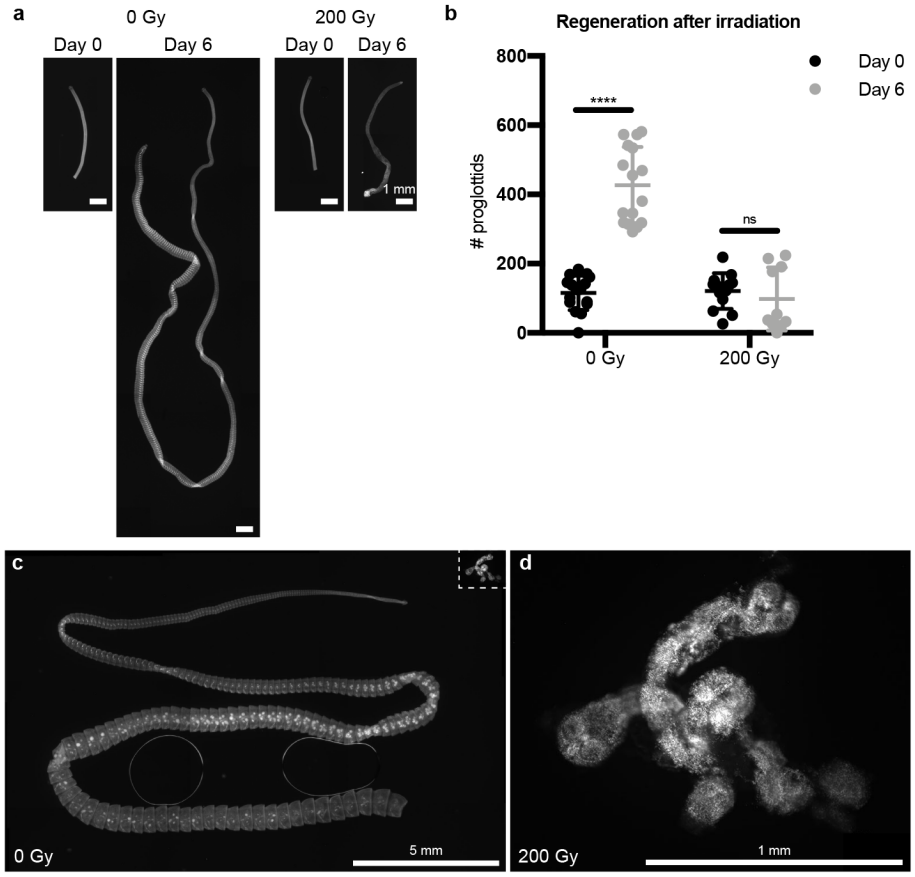

Figure 2 – figure supplement 2

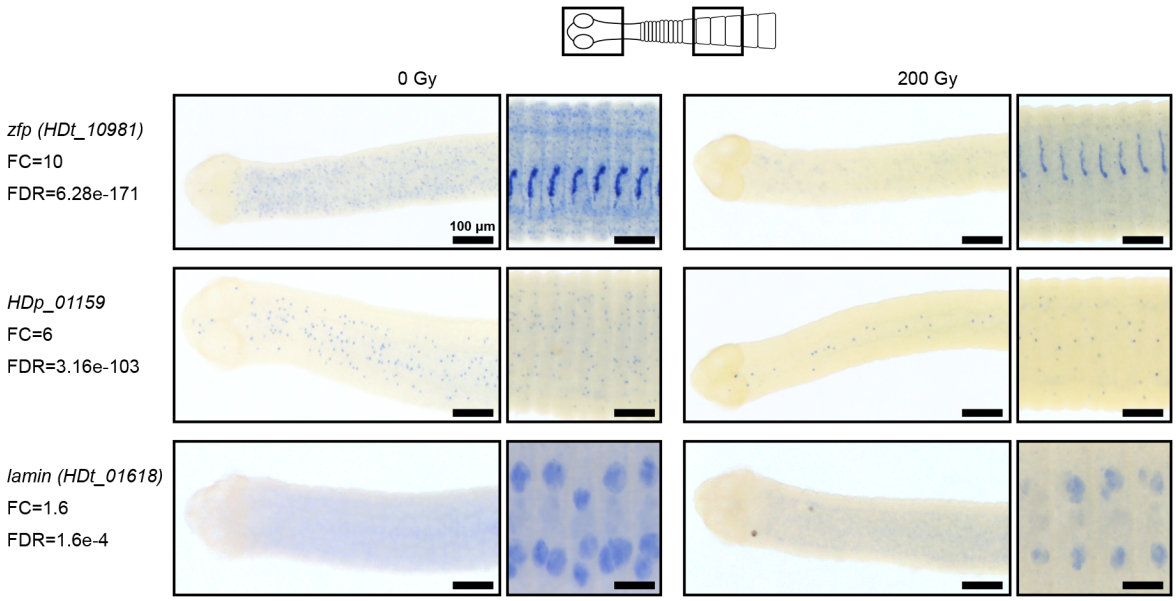

Figure 3 – figure supplement 1

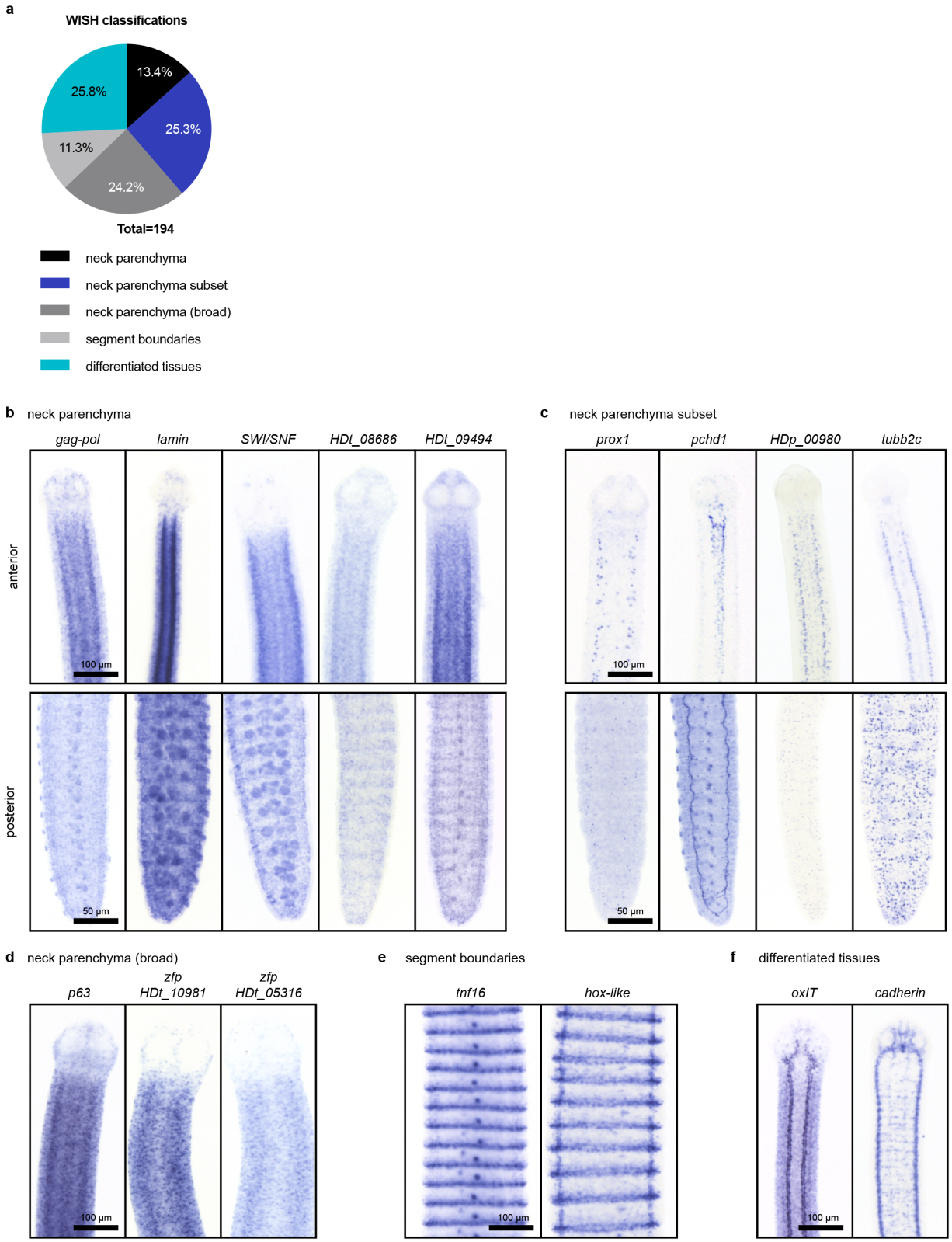

Figure 3 – figure supplement 2

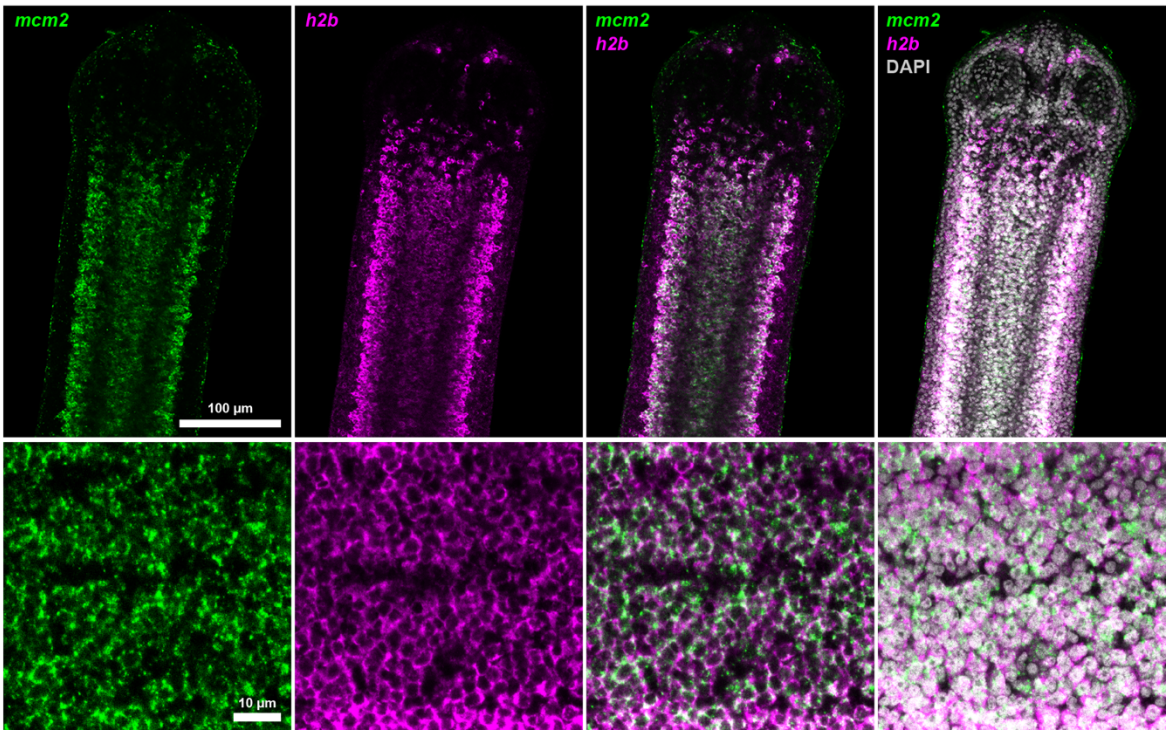

Figure 3 – figure supplement 3

a

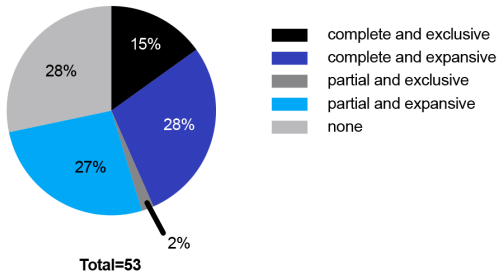

b partial and exclusive

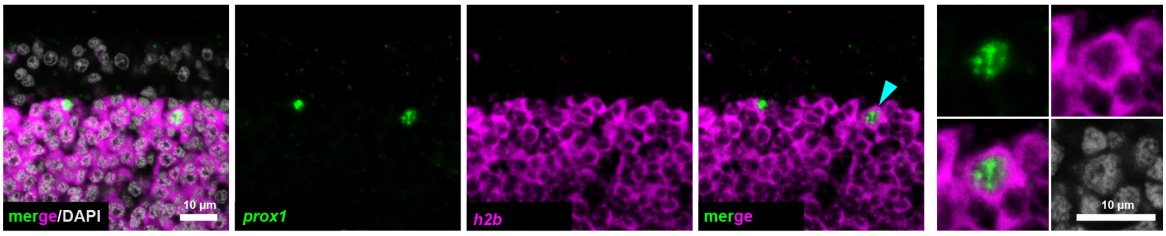

c partial and expansive

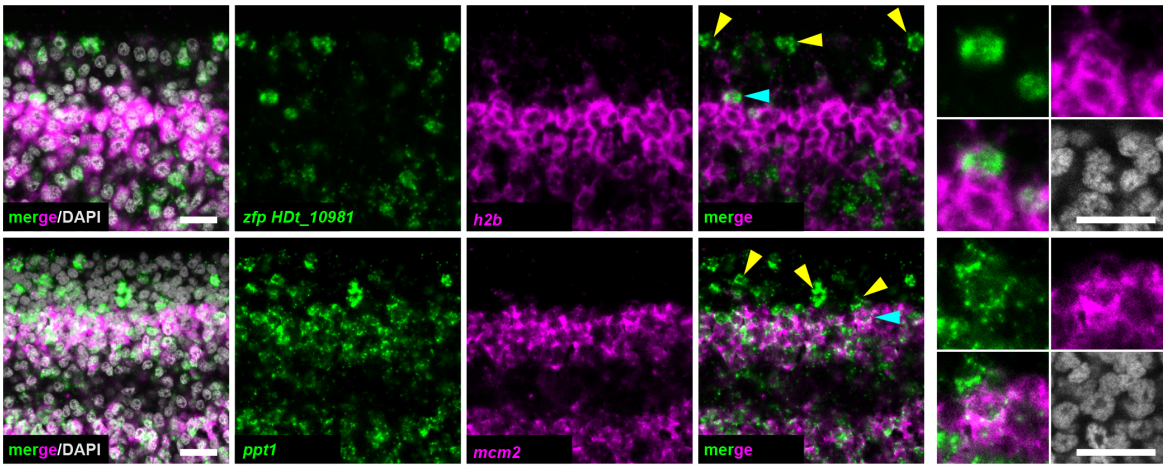

d none

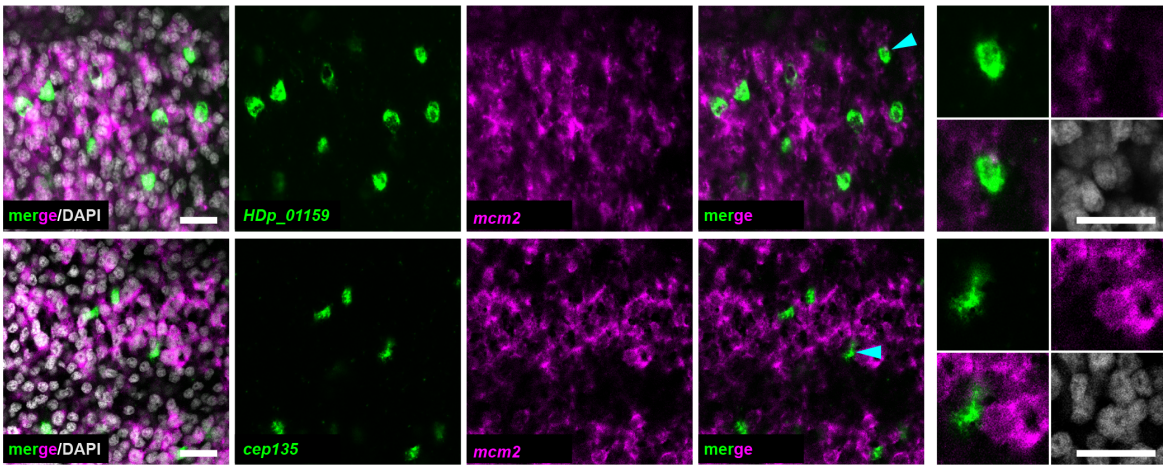

Figure 4 – figure supplement 1

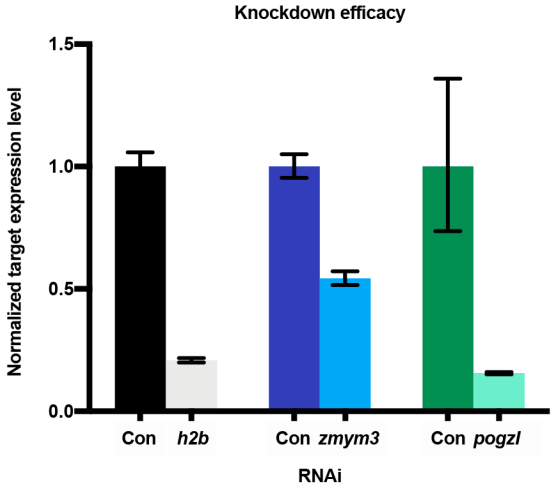

Figure 4 – figure supplement 2

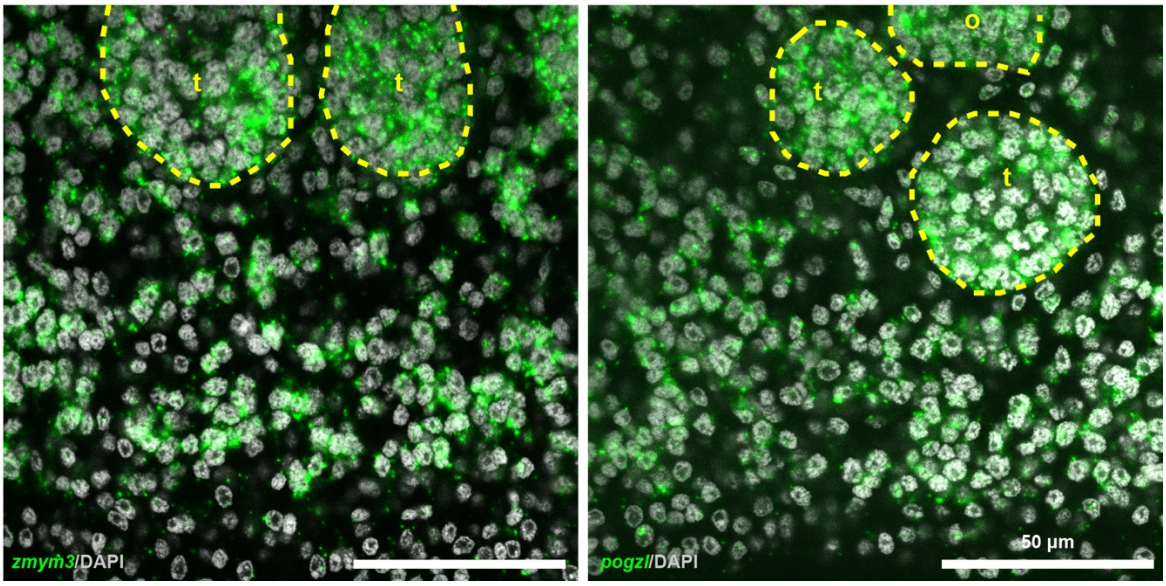

Figure 6 – figure supplement 1

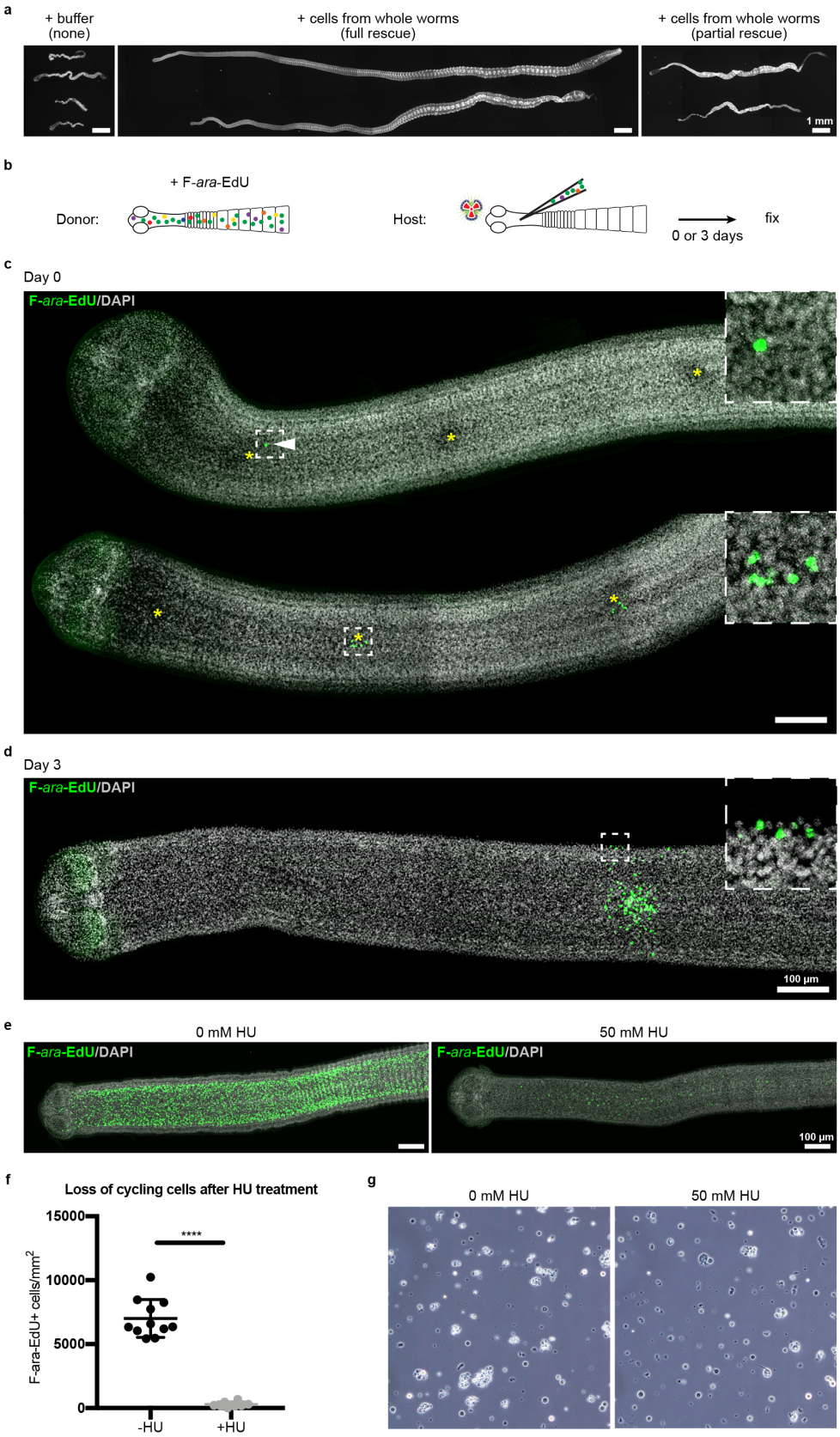
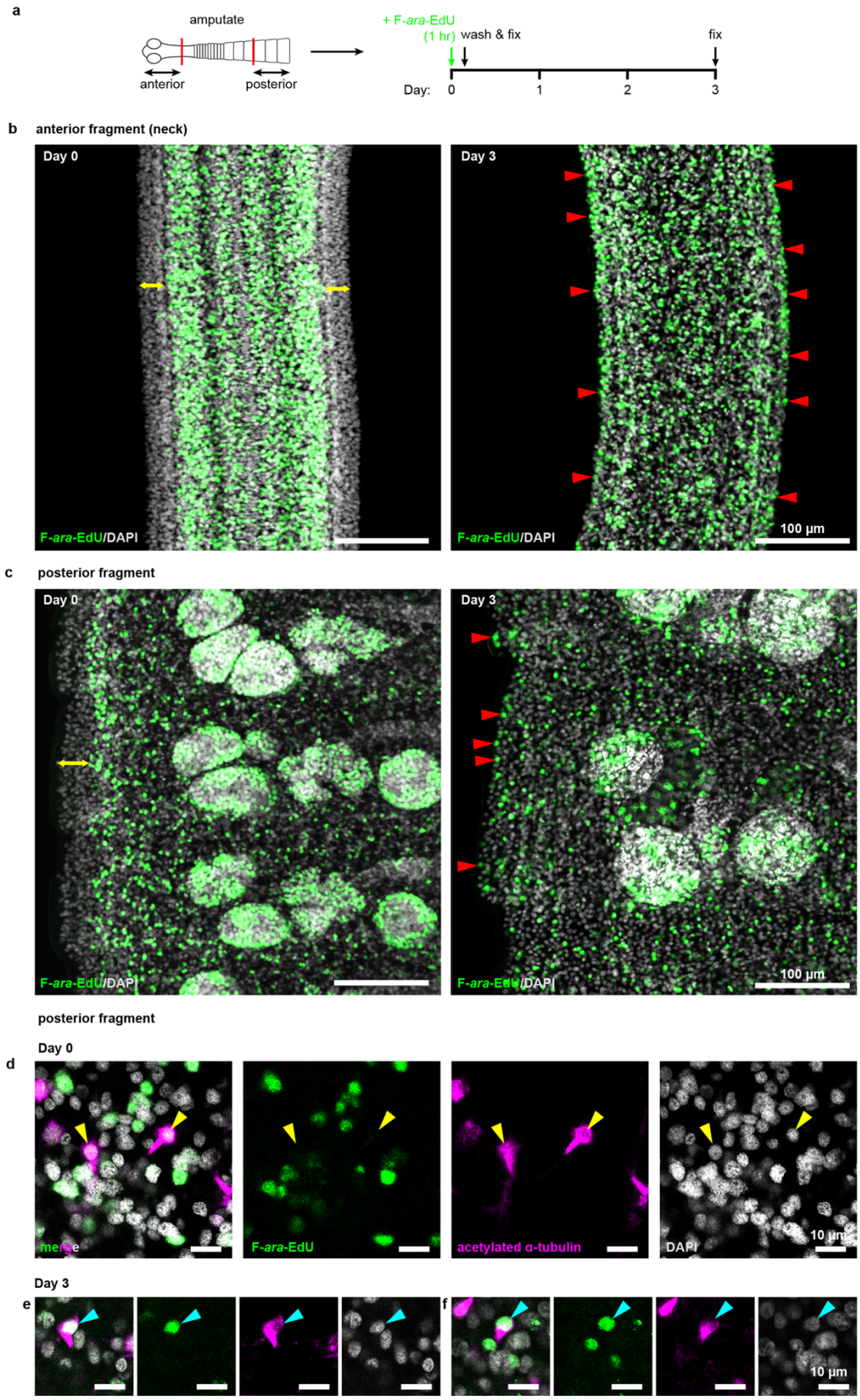
Figure 6 – figure supplement 2